SEARCH FOR PAIR PRODUCTION OF A HEAVY QUARK DECAYING INTO TOP QUARK AND PHOTON IN SEMI-LEPTONIC CHANNEL WITH THE CMS DETECTOR IN THE LHC

A THESIS SUBMITTED TO
THE GRADUATE SCHOOL OF NATURAL AND APPLIED SCIENCES
OF
MIDDLE EAST TECHNICAL UNIVERSITY

BY

ECE AŞILAR

IN PARTIAL FULFILLMENT OF THE REQUIREMENTS
FOR
THE DEGREE OF MASTER OF SCIENCE
IN
PHYSICS

JULY 2014

Approval of the thesis:

SEARCH FOR PAIR PRODUCTION OF A HEAVY QUARK DECAYING INTO TOP QUARK AND PHOTON IN SEMI-LEPTONIC CHANNEL WITH THE CMS DETECTOR IN THE LHC

submitted by **ECE AŞILAR** in partial fulfillment of the requirements for the degree of **Master of Science in Physics Department, Middle East Technical University** by,

Prof. Dr. Canan Özgen _____
Dean, Graduate School of **Natural and Applied Sciences**

Prof. Dr. Mehmet Zeyrek _____
Head of Department, **Physics**

Prof. Dr. Ali Murat Güler _____
Supervisor, **Physics Department, METU**

Examining Committee Members:

Prof. Dr. Ramazan Sever
Physics Department, METU _____

Prof. Dr. Ali Murat Güler
Physics Department, METU _____

Prof. Dr. Orhan Çakır
Physics Department, AU _____

Prof. Dr. Altuğ Özpineci
Physics Department, METU _____

Prof. Dr. Osman Yılmaz
Physics Department, METU _____

Date: _____

I hereby declare that all information in this document has been obtained and presented in accordance with academic rules and ethical conduct. I also declare that, as required by these rules and conduct, I have fully cited and referenced all material and results that are not original to this work.

Name, Last Name: ECE AŞILAR

Signature :

ABSTRACT

SEARCH FOR PAIR PRODUCTION OF A HEAVY QUARK DECAYING INTO TOP QUARK AND PHOTON IN SEMI-LEPTONIC CHANNEL WITH THE CMS DETECTOR IN THE LHC

Aşılar, Ece
M.S., Department of Physics
Supervisor : Prof. Dr. Ali Murat Güler

July 2014, 52 pages

In this thesis, a search for a pair produced excited quark, t^*, which decays exclusively to a top quark and a photon, is performed by considering semi-leptonic decay channel. This entails that there are two isolated photons, at least 4 well-reconstructed jets and one lepton, which can be either a single isolated muon or electron, in the final state. Moreover, the χ^2 sorting method and matrix method is presented to reconstruct signal and to determine fake rate of photons coming from leptons and jets, for background reconstruction, respectively. Tag and Probe method and QCD-enriched samples are also implied to make use of matrix method. In this study, proton-proton collision data collected by CMS at 8 TeV corresponding to an integrated luminosity of $19.6 fb^{-1}$ is investigated. Analysis is performed in a model independent way while a heavy spin-3/2 excitation of a heavy spin-1/2 quark indicated by "Rarita-Schwinger" vector spinor Lagrangian is the most favorable choice among other beyond the standard models. As a result of this study, no significant excess is observed over expectations and a

lower limit is set on a t* quark mass of 969 GeV/c^2 at 95% confidence level.

Keywords: LHC, CMS, Heavy Quark, Extra Dimensions, Randall Sundrum Model, Warped Geometry

ÖZ

LHC'DE CMS DENEYİNDE TOP KUARK VE FOTONA BOZUNAN YENİ AĞIR KUARKIN YARI LEPTONIK KANALDA ÇIFT URETILMESININ ARAŞTIRILMASI

Aşılar, Ece
Yüksek Lisans, Fizik Bölümü
Tez Yöneticisi : Prof. Dr. Ali Murat Güler

Temmuz 2014 , 52 sayfa

Bu tezde LHC'de CMS deneyinde top ve foton rezonansı çalışıldı. Temel olarak top kuark üzerine yoğunlaşılırken analiz herhangi bir modele dayanmamaktadır. Çift olarak üretilen yeni ağır kuarkın top kuark ve fotona gittiği kanal yarı leptonik olarak çalışıldı. Bu da son durumda iki foton, bir muon veya bir elektron ve en az dört iyi tespit edilmiş jetin varlığını gösterir. Kanal araştırılırken iki temel yöntem kullanıldı. Sinyal bölgesi saptaması için χ^2 elemesi kullanılırken ardalanın belirlenmesi için Matris metodu kullanıldı. Matris metodunda etiketle-ölç tekniği ve zenginleştirilmiş KRD veri örneği ile yapılan çalışmalar önemli rol oynadı. Bu araştırmada 19.6 fb^{-1} toplam ışınlığa denk gelen 8 TeV çarpışma verisi incelenmiştir. Sonuç olarak, beklentilerin üzerinde bir sapma gözlenmemesinin yanında yeni ağır kuark kütlesinin alt sınırı %95 güven seviyesinde 969 GeV/c^2 olarak belirlendi.

Anahtar Kelimeler: BHC, CMS, Ağır Kuark, Ek boyutlar, Randall Sundrum Model, Çarpık Uzay

To my mother and brother

Şenay Özçiftçi, Mehmetefe Aşılar

ACKNOWLEDGMENTS

First of all, I would like to thank to my supervisor Prof. Dr. Ali Murat Güler for his continuous support and for giving me the great opportunity to work at CMS at CERN.

I would like to thank all my collaborators at CMS especially to Yeng-Ming Tzeng (Jacky), and Shin-Shan Yu (Eiko) for accepting me in their group. I would also like to thank Marco Cardaci for his endless support during this search. I managed to develope a tag and probe code and calculate fake rate from leptons with his help. His logical thinking, patience and enthusiasm have been great motivation for me. He has been such a wonderful mentor to me. I like also to thank Yu-Hsian Chang and Kai-Feng Chen without them it would be impossible to finalize this search.

I would also like to thank the rest of my thesis examining committee: Prof. Dr. Orhan Çakır, Prof. Dr. Altuğ Özpineci, Prof. Dr. Ramazan Sever, Prof. Dr. Osman Yılmaz.

In addition, I like to thank Prof. Mithat Kaya and Özlem Kaya, Cemali Kılınç, Metin Yalvaç, Buğra Bilin, Merve Demirtaş for their friendship.

My sincere thanks also goes to Gokhan Alkaç for his many scientific advices and close friendship during my undergraduate and graduate education.

I am thankful to all my friends particularly Özlem Yavaş, Hakan Keskin and Zeynep Özer for their motivations and many helpful discussions.

Furthermore, I would like to thank my mother and brother for supporting me materially and spiritually throughout my life.

Finally, this thesis work is financially supported by Turkish Atomic Energy Agency with Project No: CERN-A5.H2.P1.01-06.

TABLE OF CONTENTS

LIST OF TABLES

TABLES

LIST OF FIGURES

FIGURES

LIST OF ABBREVIATIONS

ALICE	A Large Ion Collider Experiment
ATLAS	A Toroidal LHC Apparatus
BSM	Beyond the Standard Model
CM	Center of Mass
CMS	Compact Muon Solenoid experiment
CMSSW	CMS SoftWare framework
DAQ	Data Acquisition
ECAL	Electromagnetic Calorimeter
HCAL	Hadron Calorimeter
HF	Hadron Calorimeter (Forward)
LHC	Large Hadron Collider
LHCb	the Large Hadron Collider Beauty Experiment
LINAC	Linear particle Accelerator
PDG	Particle Data Group
QFT	Quantum Field Theory
RFQ	Radio Frequency Quadrupole
RS	Randall Sundrum
SM	Standard Model

CHAPTER 1

INTRODUCTION

This study puts into limelight the top quark and photon physics at CMS. The former, top quark was discovered as the sixth missing quark to complete the three generations of the Standard Model(SM), in 1994. Since then experimental precision has been advanced so that the top quark mass is measured as 173.5 $\pm$ 0.6 $\pm$ 0.8 GeV/c^2 (June 2012 PDG value) [1]. Due to heaviness of top quark many models foresee that top quark is a composite particle rather than an elementary one [2, 7]. As for the latter, the photon is important because γ+jets and $\gamma\gamma$ processes are background to Higgs searches and searches beyond the standard model(BSM). Besides this, CMS detector has a very comprehensive Electromagnetic calorimeter (ECAL) and therefore di-photon mass resolution is very precise, namely about 1% at 100 GeV.

Although SM has a proven success in describing the current data, it still has some theoretical shortcomings which will be explained in a more detailed fashion in Section 1.1.1.1. One of these inadequacies is called the hierarchy problem which concerns large energy difference between Electroweak scale and Plank scale. The Randall-Sundrum(RS) [8, 9] Model solves the hierarchy problem by introducing extra-dimensions that gravity can penetrate into. Thus, one possibility for t^* is to be a spin-3/2 Regge excitation in RS model. Moreover, since a resonance of t + γ has not been probed in CMS yet, it is essential to look for pair production of heavy quark decaying into top quark and a photon semi-leptonically.

For this analysis, it is assumed that $t^*\rightarrow t+\gamma$ has a 100% branching fraction as it is dominant channel over $t^*\rightarrow t + g$ and $t^*\rightarrow t + Z$. Only pair production

of t^* is considered because it has a higher production cross section than single production of t^* at the LHC. This is due to the fact that mixing between spin-3/2 and spin-1/2 states is suppressed [10]. Although a spin-3/2 RS resonance is focussed, the analysis is performed in a model independent way. The semi-leptonic decay channel of the system is taken under consideration, i.e. $t \to bW$ with $W \to qq$ on one side and $W \to \ell\nu$ on the other side, where ℓ maybe either an electron or a muon.

The main motivation of this search is to find t^* particle in other words to measure excess of events consistent with t^* pair production more than 3σ to claim as a discovery. In case the particle couldn't be found, a lower limit on mass of t^* would be determined.

This thesis is mainly divided in three parts. The first chapter, which is introduction, explains the theory behind this research. The following chapter is reserved for the experimental setup which is CMS detector and the LHC. The subsequent chapter, chapter three, is dedicated to analysis part which contains χ^2 sorting method in order to reconstruct signal and matrix method to describe background. At the end, forth chapter, conclusions will be discussed.

1.1 Theory

1.1.1 Standard Model

Nowadays, the Standard Model (SM) (see [11] for a pedagogical introduction) is the most comprehensive model which describes the subatomic particles and their interactions (Table 1.1). In SM, there are two types of subatomic particles, fermions and bosons. Fermions have half integer spin and therefore they obey the Pauli Exclusion Principle; two fermions can not stay in the same quantum state simultaneously. This phenomenon is known as Fermi-Dirac statistics. In Table 1.1 one can see 12 fundamental particles which imply that they can not be subdivided into smaller particles. It should be noted that all visible matter in the universe is formed of these 12 particles. Moreover, these particles have partners which are particles with the same mass, but opposite electromag-

netic charge, color and opposite component of the weak isospin. These pairs are called antiparticles. On the other hand, bosons have an integer spin and obey the Bose–Einstein statistics which allows particles aggregation in the same state. According to SM, bosons are force carriers of corresponding interaction which is shown in the Table 1.2. In the Table, interactions are written with respect to their strength. The range of interaction is inversely proportional to mass of intermediate boson; However, due to self interaction of gluons strong force behaves differently. Gluons are mediators of Strong force and couple to color charge. The coupling strength of Strong force is decreasing with the increasing energy which is called "asymptotic freedom" [12]. It is impossible to give enough energy to separate a quark-antiquark pair without producing a new quark-antiquark pair. The mediator of electromagnetic interactions is photon. Charged particles, for example electrons and muons interact with photon. Weak interaction has three mediators, $W^{\pm}$ and Z. It has very low range ($10^{-18}m$) because of mediating bosons have large mass. In addition to these forces, there is Gravity in the Universe; however SM does not include. Since the Gravity is weakest force, it does not play an important role in sub-atomic level.

Table1.1: Fundamental particles of the Standard Model. Q is the electric charge of the particle

	1.Gen.	2.Gen.	3.Gen.	Q	Force
Leptons	$\binom{\nu_e}{e}$	$\binom{\nu_\mu}{\mu}$	$\binom{\nu_\tau}{\tau}$	$\binom{0}{1}$	$\binom{weak}{em,weak}$
Quarks	$\binom{u}{d}$	$\binom{c}{s}$	$\binom{t}{b}$	$\binom{+2/3}{-1/3}$	em, $weak$, $strong$

$$SU(3)_C \otimes SU(2)_L \otimes U(1)_Y \tag{1.1}$$

SM is a relativistic quantum field theory invariant under the local gauge transformation group in Equation 1.1, where $SU(3)_C$ represents a symmetry group for strong interaction while $SU(2)_L \otimes U(1)_Y$ stands for the group describing the electroweak interactions.

Table1.2: Except gravitation, all forces and their intermediate bosons are described by the Standard Model

Interaction	Coupling with	Intermediate boson	Boson mass (in GeV)	Range(m)
strong	color	8 gluons(g)	0	10^{-15}
electromag.	el.charge	photon(γ)	0	∞
weak	weak charge	$W^{\pm}, Z^0$	80,90	10^{-18}
gravitation	mass	graviton(G)	0	∞

$$Y = 2(Q - I_3) \tag{1.2}$$

In 1961, Glashow introduced that there are three conserved weak currents related to the generators of the weak isospin group $SU(3)_C$ and one to the weak hypercharge group $U(1)_Y$. A combination of two $SU(2)_L$ currents identifies charged weak currents, while a mixing of the $SU(2)$ and $U(1)$ currents indicates the neutral weak and the electromagnetic currents. The weak hypercharge is defined as in the Equation 1.2 where Q is the electric charge and I_3 is the third component of the weak isospin I.

In the Table 1.2, one can easily see that $W^{\pm}, Z^0$ bosons have masses in order to explain short range of weak interaction. However, if explicit mass terms are implemented to SM, it losses the gauge invariance and thus the renormalizability of the field theory. At this point Higgs mechanism takes care of this mass problem by introducing spontaneous symmetry breaking [13]. In the Standard Model, when the Weak and Electromagnetic forces are unified it results in three W bosons and B^0 boson which are gauge bosons mediating electroweak interaction. However, these Gauge bosons can not be observed physically. Z and γ bosons can be formed by electroweak symmetry breaking, B^0 and W^0 mix via weak angle. This relation can be seen from Equation 1.3.

$$\begin{pmatrix} \gamma \\ Z \end{pmatrix} = \begin{pmatrix} cos\theta_W sin\theta_W \\ -sin\theta_W cos\theta_W \end{pmatrix} \begin{pmatrix} B^0 \\ W^0 \end{pmatrix} \tag{1.3}$$

In Addition, $W^{\pm}$ is the superposition of W^1 and W^2 gauge bosons. This symmetry breaking also propounds the Higgs boson. In 2012, the CMS [14] and ATLAS [15] experiments at the LHC discovered a new boson which is consistent with predicted Higgs boson within SM.

1.1.1.1 Shortcomings of Standard Model

The SM is in a well consistency with current experimental data obtained from particle accelerator experiments. Considering this, SM still have some theoretical inadequacies that a fundamental theory should not involve.

Astrophysical and cosmological measurements provide evidence of Dark Matter [16, 18] which is not reactant to light. Since SM does not explain Dark Matter it need to have some extensions. Additionally, SM does not involve the non-zero neutrino masses which are essential to explain neutrino oscillations. Moreover, in SM the gauge couplings do not meet at the same point and therefore gauge coupling unification is not permitted. In addition to these, there are two hierarchy problems of SM. The first one is called the little hierarchy problem. The problem is that Quantum Field Theory (QFT) correction terms of free Higgs mass are almost equal to Higgs mass itself. One of the candidate BSMs to solve this problem is the Little Higgs model [19]. The model professes that the problem can be solved by adding new particles. These loop contributions are quadratically divergent and they are mostly coming from the loops involving top quark. The problem concerned in this thesis actually the large hierarchy problem of SM. This problem occurs due to a large energy difference between electroweak scale and Plank scale where electroweak scale is the scale at which the symmetry between electromagnetism and the electroweak interaction is broken and Plank scale associated with gravity [20]. In other words, the electroweak force is 10^{32} times stronger than gravity and SM can not explain this. The problem can be solved by RS Model [8, 9] by a string theory inspired context.

1.1.2 The Randall-Sundrum Model

Generally, it is supposed that the universe, we live in, has 3 spatial dimensions. However, it is not have to be like that. Extra spatial dimensions is introduced to unify four fundamental forces by Gunnar Nordström, in 1914. He asserted a five dimensional theory to combine electromagnetism and a scaler version of gravity. The idea [21] was further detailed by Theodor Kaluza and Oscar Klein after the development of general relativity. Although the Kaluza-Klein theory was not successful in unifying all forces, that time not all forces were discovered, subsequently many models with extra spatial dimensions have been proposed. The sizes of the extra dimensions are near the Planck length($1.616252\text{x}10^{-35}$m). Thus, it is impossible to measure experimentally with the current particle accelerators. Fortunately, a solution to this problem is provided by recent models. They propose extra dimensions large enough to be experimentally probed by current accelerators such as the LHC. One of the most widely investigated of these models is Randall-Sundrum model.

In RS Model, extra-dimensions are bounded by two branes [22] as in the Figure 1.1. In [22], also exponential dependence of the electroweak scale to the Planck scale according to TeV$\sim e^{ky} M_{Pl}$ is shown in a detailed way. Figure 1.1 shows that objects are much lighter in TeV scale because gravity confined in Plank scale.

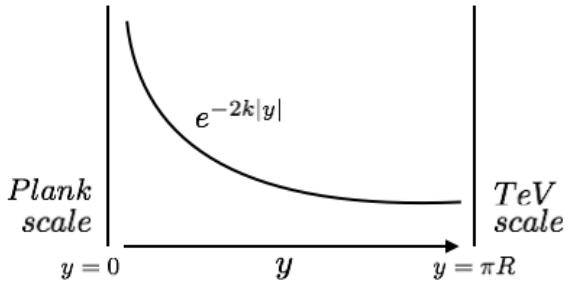

Figure 1.1: Diagram of the RS spacetime. [22]

In this thesis, t^* is considered as a spin-3/2 Regge excitation described by a Randall-Sundrum scenario given in [20]. It is described by the Lagrangian

given in Equation 1.4 [23], where $\mathcal{D}_\nu = \partial_\nu - ig\mathcal{A}_\nu$. The Lagrangian describes the interaction between the particles considered in this thesis. It can be understood from the Lagrangian there are two quarks and a photon at the same space-time point.

$$\mathcal{L}_4 \ = i\overline{\Psi_\mu}\gamma^{\mu\nu\rho}\mathcal{D}_\nu\Psi_\rho + \mathcal{M}\overline{\Psi_\mu}\gamma^{\mu\rho}\Psi_\rho \tag{1.4}$$

For $t^*\rightarrow t+\gamma$ analysis, it is assumed that it has 100% branching fraction over other channels such as $t^* \rightarrow t + Z$ and $t^* \rightarrow t + g$. Only pair production of t^* is considered because it has a higher production cross section than single production of t^* at the LHC. The reason for this is suppression of mixing between spin-3/2 and spin-1/2 states [20, 24]. It should be noted that despite consideration of a spin-3/2 RS resonance, the analysis is performed in a model independent way.

CHAPTER 2

EXPERIMENTAL SETUP

2.1 LHC

LHC [25] is the worlds highest energy accelerator with its 27 km circle which is designed to accelerate protons up to a center of mass energy 14TeV. The source of protons in the LHC is a tube of hydrogen gas. After protons are separated from hydrogen gas, they are send to a Duoplasmatron to be accelerated to energy of 90 keV. Then they start their journey with entering radio frequency quadrupole (RFQ) and continue with LINAC2 here they reach up to 50 MeV. After then they enter PS (1.4 GeV $\rightarrow$ 26 GeV) then in to SPS (26 GeV $\rightarrow$ 450 GeV). After this step they reach sufficient energy to enter LHC. With LHC, protons reach 8 TeV CM energy to simulate the similar state after the big bang. One can see schema of this journey in Figure 2.1 . Two high-energy particle beams traveling at the speed 0.99999991c are focussed, bent and accelerated simultaneously during their journey.

The particle beams collide at 4 interaction points in the LHC. These points contain also the 4 main detectors of LHC : A Large Ion Collider Experiment (ALICE), A Toroidal LHC Apparatus (ATLAS), Compact Muon Solenoid (CMS) and the Large Hadron Collider Beauty Experiment (LHCb).

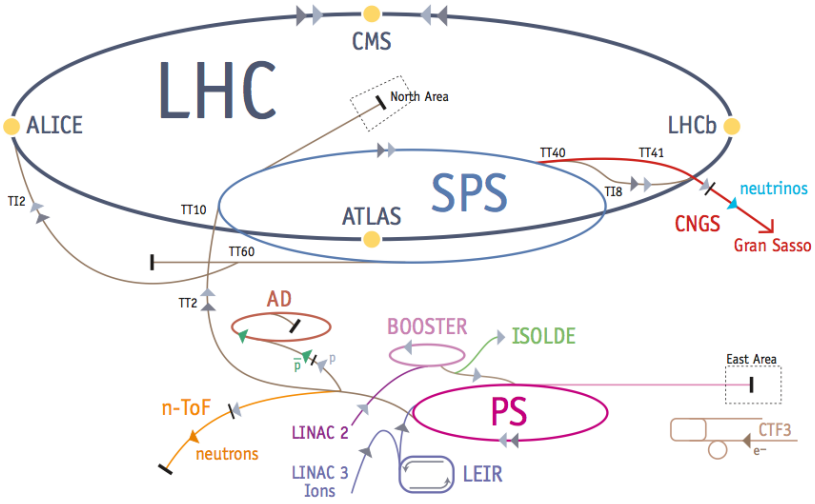

Figure 2.1: LHC complex. [25]

2.2 CMS

CMS [26, 27] is one of the two general purpose detectors of LHC. That is physics at the TeV scale, Higgs boson, BSM physics can be studied with CMS.

CMS is an onion shape detector. Main components of the detector can be seen in the Figure 2.2. A superconducting magnet (4T) is covering inner tracker and 2 calorimeters because large bending power is necessary in order to measure precisely the momentum of high-energy charged particles.

In this point it is useful to explain CMS general geometry in other words coordinate system. The proton beam line is along the Z-axis which points tangentially with respect to center of LHC circle. Y-axis is vertical and points up. Because of the ring shape of LHC and cylindrical structure of CMS it is essential to use a different kinematic variable called pseudo-rapidity;

$$\eta = -\ell n[\tan(\frac{\theta}{2})] \tag{2.1}$$

It is important to introduce η to explain barrel, endcap and forward regions of the detector. In addition to η there is one more variable ΔR to determine

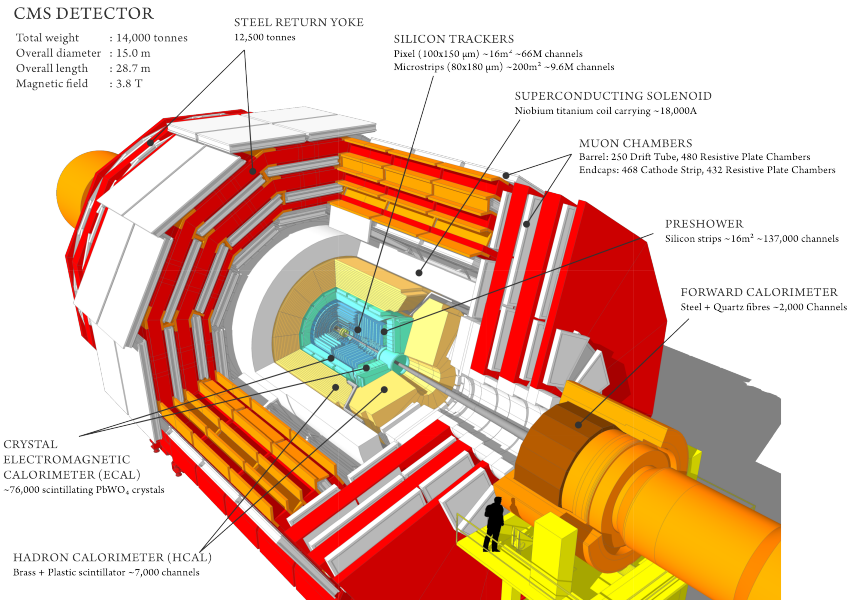

Figure 2.2: Schematic view of the CMS detector. [26]

angular distance. ΔR can be defined as a combination of distance between azimuthal angle(ϕ) and (η);

$$\Delta R = \sqrt{(\Delta\eta)^2 + (\Delta\phi)^2} \tag{2.2}$$

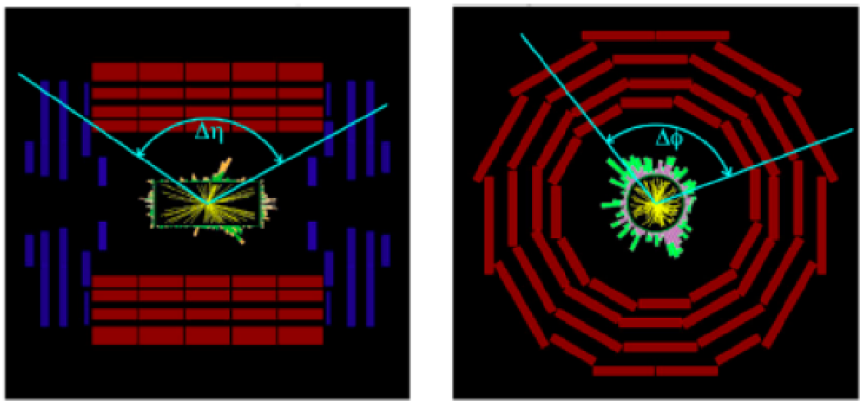

Figure 2.3: Definition of azimuthal angle(ϕ) and (η).

Since there is no instrument along the beam line, z component of particle momenta can only be measured indirectly.

2.2.1 Inner Tracking System

The innermost detector component is Tracker made entirely of silicon. In Figure 2.4 , there are 3 layers of pixel detector (in purple), 10 layers of silicon microstrip detectors (in red and blue) in the central region and 2 layers of pixel, 12 layers of silicon microstrip detectors in the endcaps to provide a good resolution. Transverse impact parameter resolution of charged particles reaches 10μm for high P_T tracks. Thus, CMS tracker is very good at determining the position of secondary vertices which is important to tag b jets.

For this analysis tracker has an important role in determining leptons P_T and it is also important to measure jet energies by matching associated tracks.

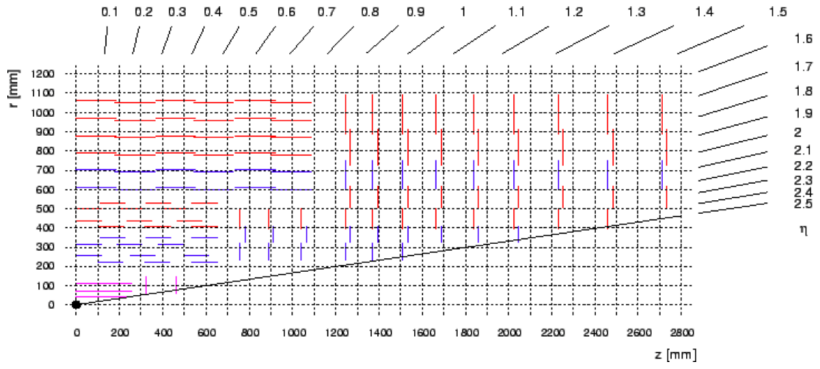

Figure 2.4: One quarter of the CMS Tracker layout. [28]

2.2.2 Electromagnetic Calorimeter

The electromagnetic calorimeter (ECAL) has pseudo-rapidity $|\eta| < 3$ and measures energy of the particles interacting electromagnetically like electrons and photons which play an important role in this analysis. In order to measure energy precisely ECAL is composed of 61200 lead tungstate (PbWO4) crystals. These crystals with their characteristics permit a fine granularity and compactness [29]. The region with $|\eta| < 1.48$ is reserved for the ECAL barrel (EB) and The ECAL endcaps (EE) positioned in the region $1.48 < |\eta| < 3.0$.

The energy resolution of both EB and EE is given by Equation 2.3.

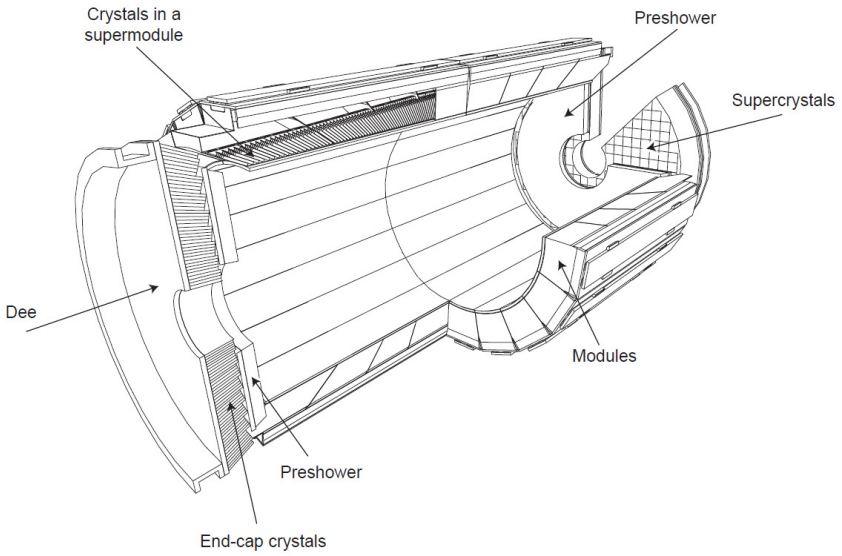

Figure 2.5: Layout of the CMS electromagnetic calorimeter presenting the arrangement of crystal modules, supermodules, endcaps and the preshower in front [29].

$$(\frac{\sigma}{E})^2 = (\frac{S}{\sqrt{E}})^2 + (\frac{N}{E})^2 + C^2 \tag{2.3}$$

(S) is called the stochastic term presenting the event-to-event fluctuations, photoelectron statistics, and other fluctuations in the energy deposited in the preshower absorber. (N) is the noise term corresponding to electronic, digitization, dark current and pileup noise. The light collection non-uniformity, errors on the inter-calibration among the modules, and the energy leakage from the back of the crystal are shown with the constant term (C). Also, it should be noted that E is in GeV. For example in 2004 barrel supermodule was tested with an electron beam having momenta between 20 and 250GeV/c. As a result of this test S,N,C were estimated as 2.8%, 0.12, 0.30% respectively.

2.2.3 Hadron Calorimeter

ECAL is surrounded by hadronic calorimeter (HCAL) which is a brass/scintillator sampling hadron calorimeter within the same pseudo-rapidity as ECAL. HCAL

is used to measure energy of the particles made of quarks and gluons. In other words, HCAL measures energy of Strongly interacting particles.

Figure 2.6 shows the longitudinal view of the CMS HCAL detector where one can easily see the locations of hadron barrel (HB), hadron outer (HO), hadron endcap (HE) and hadron forward (HF) components of the detector.

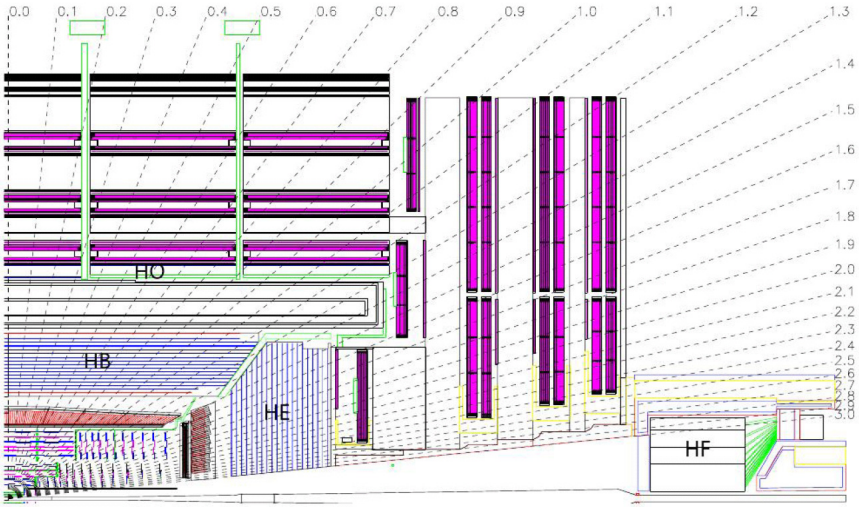

Figure 2.6: One quarter of HCAL Longitudinal view. The dashed lines are fixed η values [29].

Due to the fact that initial transverse momentum of protons is zero, it should remain zero after the collision. By considering this fact Missing Transverse Energy (MET) can be measured with the help of HCAL and ECAL [30]. Determining MET is very crucial for new physics searches and also for this search to measure the W boson mass via leptonic channel.

Measurement of direction and energy of particle jets can be also done by considering ECAL and HCAL results simultaneously [30]. The energy resolution obtained from test on combination of ECAL and HCAL is given by;

$$(\frac{\sigma}{E})^2 = (\frac{70\%}{\sqrt{E}})^2 + (8\%)^2 \tag{2.4}$$

The Equation 2.4 gives approximately 5mm width of EM shower when pion is used with energy interval from 150 to 300 GeV [29].

2.2.4 The Muon System

The outermost layer is muon chamber composed of four muon station spaced with iron "return yoke" plates. The muon chamber also is a tracking device and because it is in the outermost region of CMS no other particles except muons and neutrinos can reach this section. Thus, reconstruction of the muons are fast and highly efficient [29]. In addition to this muon charge can be determined with the help of bending direction in the magnetic field, positively and negatively charged particles are bending in opposite directions.

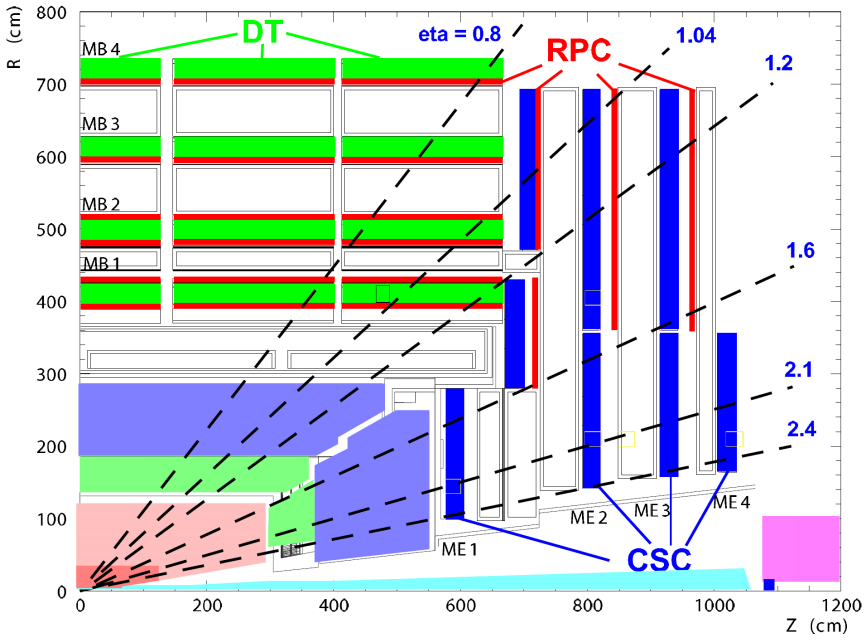

Figure 2.7: A longitudinal view of the muon system indicating the location of the three detector types of the muon system. Dashed lines represent fixed η [29].

Figure 2.7 shows the muon system of the CMS detector which is a combination of three detectors: Drift Tubes (DT), Cathode Strip Chambers (CSC) and Resistive Plate Chambers (RPC).

2.2.5 Trigger and Data Acquisition System

There are many challenges for Trigger and Data Acquisition (TDAQ) system at LHC. Some of these are enormous data rate (40 MHz per collisions), pro-

duction of approximately 20 event per bunch crossing which means 1Tbyte of zero suppressed data in CMS readout system and the cross section is very small for new physics. In order to collect data at this high rate, CMS has a complex TDAQ system as seen in the Figure 2.8 at left. On the other hand it can be explained in a simpler way as in the Figure 2.8 at right. CMS has only two trigger levels, L1 trigger and High Level Trigger (HLT). Event rate of 40 MHz is reduced to 100kHz by L1 trigger system to be passed to HLT system. There are intermediate event building step (readout buffers) and large network switching between L1 and HLT. HLT is a software system that makes event rate decreases 100Hz and this results in a data rate of 150 Mbyte per second.

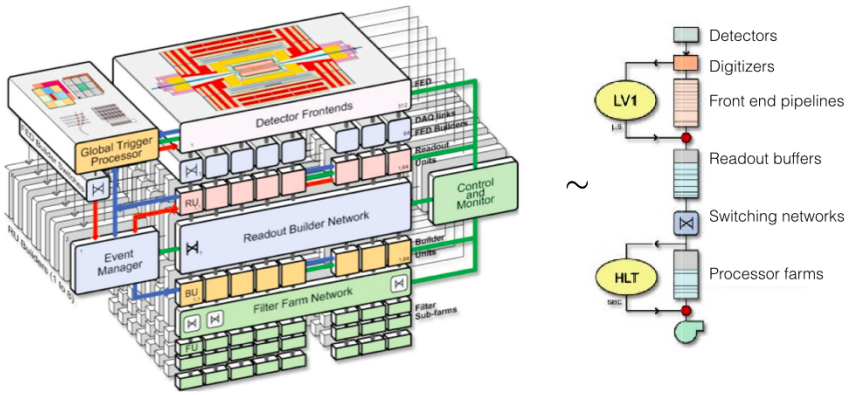

Figure 2.8: General TDAQ structure of CMS (left), summarized TDAQ structure of CMS(right) [29].

2.2.6 Computing

The most important part of the CMS computing system is CMS software (CMSSW) stands for online data taking, simulation, primary reconstruction, and physics analysis [29]. Since CMSSW composed of many subpackages related to physics analysis, complicated analysis steps become much simpler. There are also a lot of useful functions specific to CMSSW, for example CMSShape is used in this analysis to fit Background data (detailed in Section 3.3.1.1).

Some crucial steps have to be performed in order to reach data analysis stage. After filtering the first data with the help of L1 trigger and HLT, the process of selecting events and saving them in output is performed which is called

skimming. This detector output is RAW data from which the physics object reconstructed by a second skimming. Now this new data is called reconstructed (RECO) data. RECO data includes reconstructed objects such as tracks, vertices, jets, electrons, muons and hits/clusters. Moreover, there is Analysis Object Data (AOD) derived from RECO data, to provide data for physics analysis in a convenient, compact format [31]. Physics analyses can directly use AOD Data. All these RAW, RECO and AOD tiers can be seen in Figure 2.9. It should be noted that data formants of CMS are in ROOT format which is a C++ based framework for data processing.

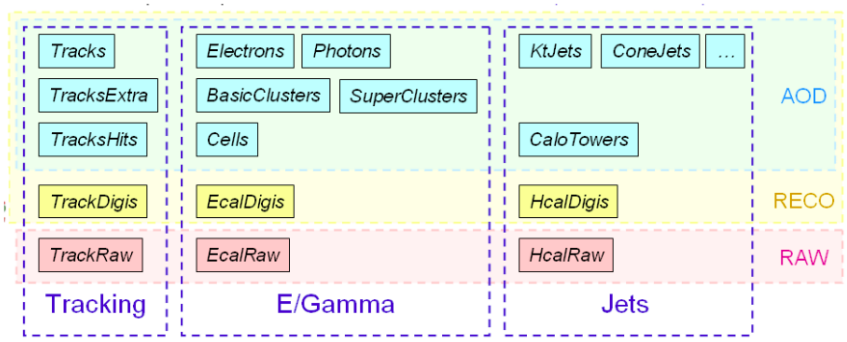

Figure 2.9: DATA tiers of CMS [31].

CHAPTER 3

ANALYSIS

In this thesis, a search for a pair produced excited quark (t^*) is performed using proton-proton collision data collected by CMS at 8 TeV corresponding to an integrated luminosity of $19.6 fb^{-1}$. In this analysis, t^* decays exclusively to a top quark and a photon. Figure 3.1 shows that analysis is performed in semi-leptonic channel. In the final state there are two isolated photons, at least 4 well-reconstructed jets and one lepton, which can be either a single isolated muon or electron. Analysis is performed in a model independent way while a heavy spin-3/2 excitation of a heavy spin-1/2 quark indicated by "Rarita-Schwinger" vector spinor Lagrangian is the most favorable choice among other beyond the standard models.

In this chapter, discussing analysis in details, Monte Carlo (MC) and data samples used in this search and corresponding computing tools will be presented. Then, χ^2 sorting and Matrix method with tag and probe technique will be explained in a detailed fashion.

3.1 MC and Data Samples

The proton-proton collision events with a CM energy of 8 TeV are used for this analysis, measured with the pixel subdetector information. These events were collected using muon or electron triggers, and reconstructed using CMS software [1]. Data Sets processed for this analysis are shown in Table 3.1.

[1] Version CMSSW_5_3_7_patch5

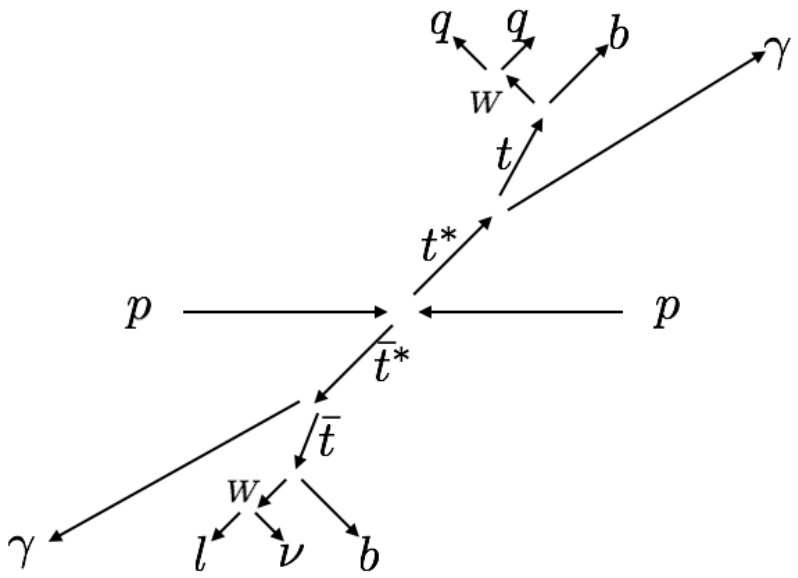

Figure 3.1: t* decays to top quark and a photon semi-leptonically.

Signal efficiencies are predicted using simulated samples. The pair production of $pp \to t^*\bar{t}^*$ signal process is simulated, including upto two additional hard partons, using the MADGRAPH [32] event generator and the CTEQ6L1 [33] parton distribution functions (PDFs) and then passed to PYTHIA [34] for hadronization. Moreover, detector simulation is performed using GEANT4 [35] in CMSSW [2].

Table3.1: Summary of 8 TeV collision data streams used in this analysis, along with their run ranges and integrated luminosity

Dataset	Run Range	$\mathcal{L}(pb^{-1})$
/MuHad/Run2012A-22Jan2013-v1	190645–193621	876.2
/SingleMu/Run2012B-22Jan2013-v1	193834–196531	4411.7
/SingleMu/Run2012C-22Jan2013-v1	198049–203002	7055.2
/SingleMu/Run2012D-22Jan2013-v1	203709–208686	7369.0
/ElectronHad/Run2012A-22Jan2013-v1	190645–193621	876.2
/SingleElectron/Run2012B-22Jan2013-v1	193834–196531	4411.7
/SingleElectron/Run2012C-22Jan2013-v1	198049–203002	7055.2
/SingleElectron/Run2012D-22Jan2013-v1	203709–208686	7369.0

[2] Version CMSSW_5_3_2_patch4

3.2 Signal Reconstruction

Event reconstruction is performed by using Particle Flow (PF) [36, 39] algorithm which combines the information of all CMS subdetectors to reconstruct and identify all stable particles in an event. The PF algorithm first reconstructs the central elements which are the charged particle tracks, calorimeter clusters, and muon tracks. Then they are linked into blocks and interpreted as particles. Since a particle can be detected in various subdetectors, the PF elements must be connected with each other, which is done with a linking algorithm to avoid double counting. The last step consists of reconstructing and identifying particles based on the blocks of elements.

3.2.1 Reconstruction of elements

- Trigger [40]: The events passing through triggers (L1 and HLT) explained in Section 2.2.5, which look for a high P_T lepton and at least three jets in an event, were analyzed.

- Primary vertex reconstruction: The presence of a primary vertex, which is consistent with the beamspot position, can indicate a collision happening. The noncollision backgrounds, such as beam halo and cosmic-ray muons, can be vetoed by requiring a primary vertex. The primary vertex can be well-reconstructed by requiring: more than 10 tracks originating from it, with at least 25% of those being high purity; at least 4 degrees of freedom; an impact parameter with respect to the beamspot in z, d_z, that satisfies $|d_z|<24$ cm; an impact parameter with respect to the beamspot in the xy plane, d_{xy}, that satisfies $d_{xy}<2$ cm.

- Lepton Reconstruction:
  Muon reconstruction and selection: Muons are initially reconstructed by identifying hits in the different layers of the muon chamber such as drift tubes and the CSCs. There are two different approaches, global muons and tracker muons, to construct straight line track segments in the local reconstruction by using hits. These tracks can be either based on hits in

the muon detector alone or a combination of hits in the muon detector with in the central detector. The latter muons are called global muons. When low P_T (<5GeV) muons are considered, using tracker muons are more efficient. On the other hand, since the algorithm makes use of full bending power of the CMS magnetic field, resolution of high P_T global muons is better. Thus, in this search muons are reconstructed as a global muon. Additionally, muons are selected with P_T >20GeV/c, $|\eta|$<2.1, tight tag of the muon physics object group (POG) [41]. Multiplicity distribution for muon is given in Figure 3.2

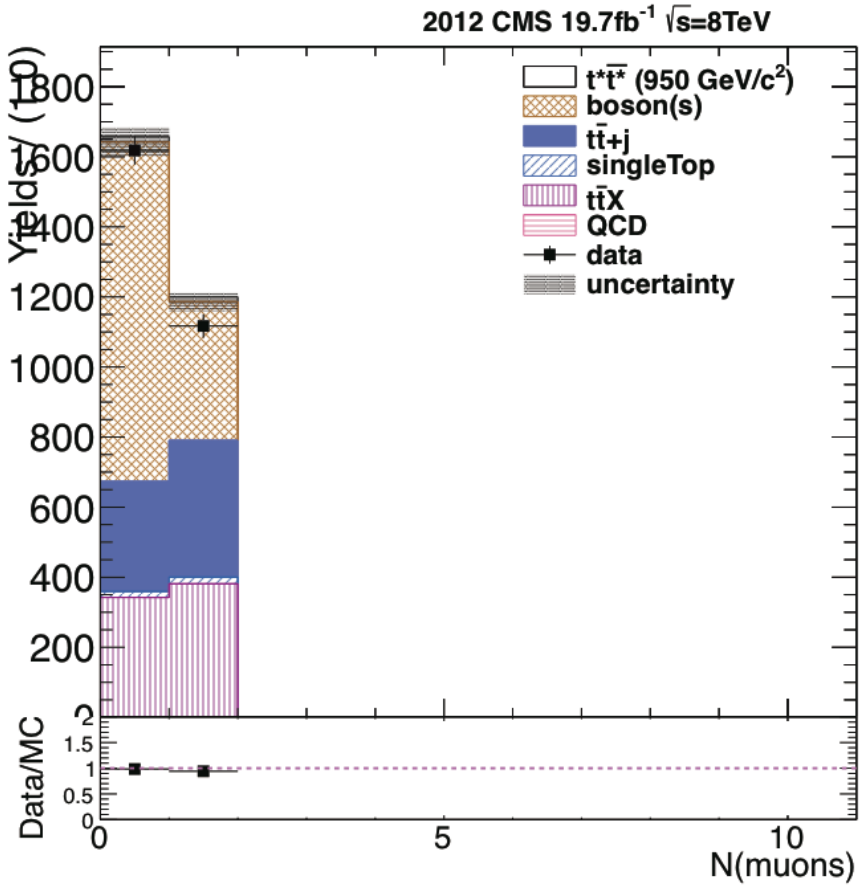

Figure 3.2: Multiplicity distribution for muon.

Electron reconstruction and selection [42]: In CMS electrons leave their signatures both in the tracker and ECAL. This signature is an energy deposit in ECAL which collects bremsstrahlung photons emitted along the electron trajectory in the tracker volume. A cluster driven pixel hit match-

ing algorithm with a Gaussian Sum Filter is used to determine energy and momentum of electron in CMS. The electron energy is deduced from a weighted combination of the corrected supercluster energy and tracker momentum measurements. The electron direction is that of the reconstructed electron track at interaction vertex. In this search, electrons tagged as tight by egamma POG are selected. Moreover, P_T >30GeV/c, $|\eta|$<2.4 cuts are applied to recontructed electrons and since there is a transition region between barrel and endcap electrons in that region (1.4442<$|\eta|$<1.566) are not taken under consideration. Multiplicity distribution for electrons is given in Figure 3.3

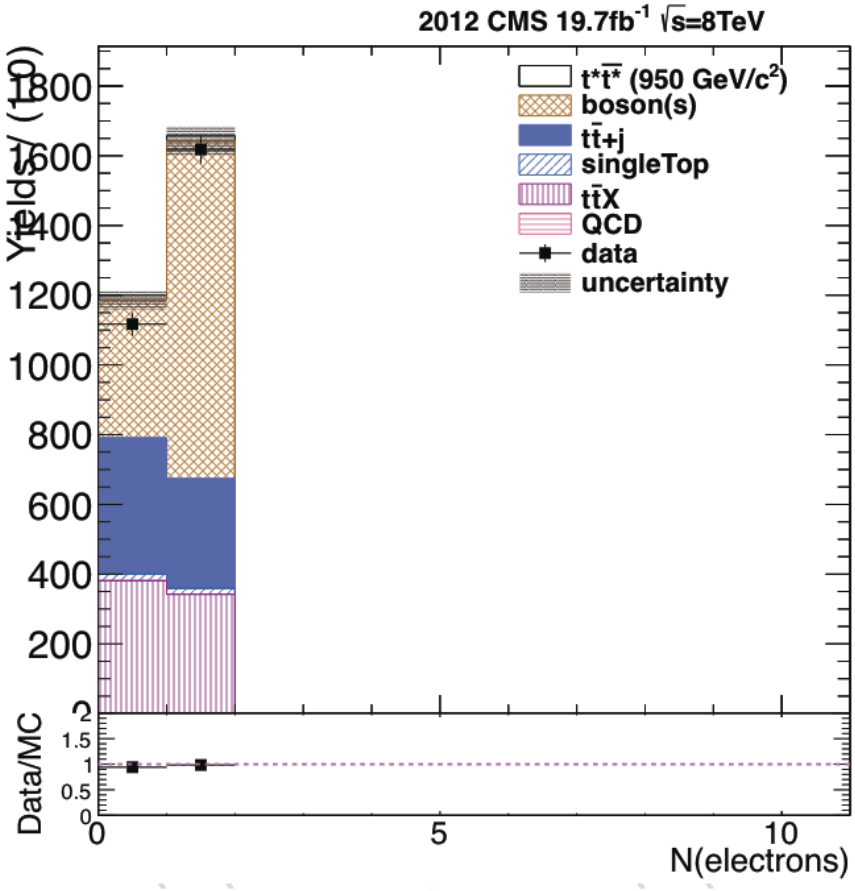

Figure 3.3: Multiplicity distribution for electron.

In addition to electron and muon selection, a simple cleaning cut is applied to distinguish electrons from muons (ΔR(muons,electrons)>0.3).

- Photon Reconstruction and Selections [43]: In this analysis, there are two

isolated photons to be reconstructed. Photons can be reconstructed with a very good energy resolution in CMS by means of the ECAL granularity, tracker, and the large magnetic field. Charge particles are bended with the magnetic field and with granularity of ECAL photons can be separated well from the charged particles. The photons identification made by egamma POG is mainly based on isolation, shower shape variables, and the ratio of energy deposits in the single hadronic calorimeter tower divided by the energy deposits in the single electromagnetic calorimeter tower (H/E). As in electron selection case, photons tagged as tight by egamma POG are selected. Moreover, P_T >30GeV/c, $|\eta|$<2.5 cuts are applied and again photons in the region 1.4442<$|\eta|$<1.566 are vetoed.

Additionally, a simple cleaning cut is applied to distinguish photons from leptons (ΔR(photons,leptons)>0.3). Multiplicity distribution for photons is given in Figure 3.4.

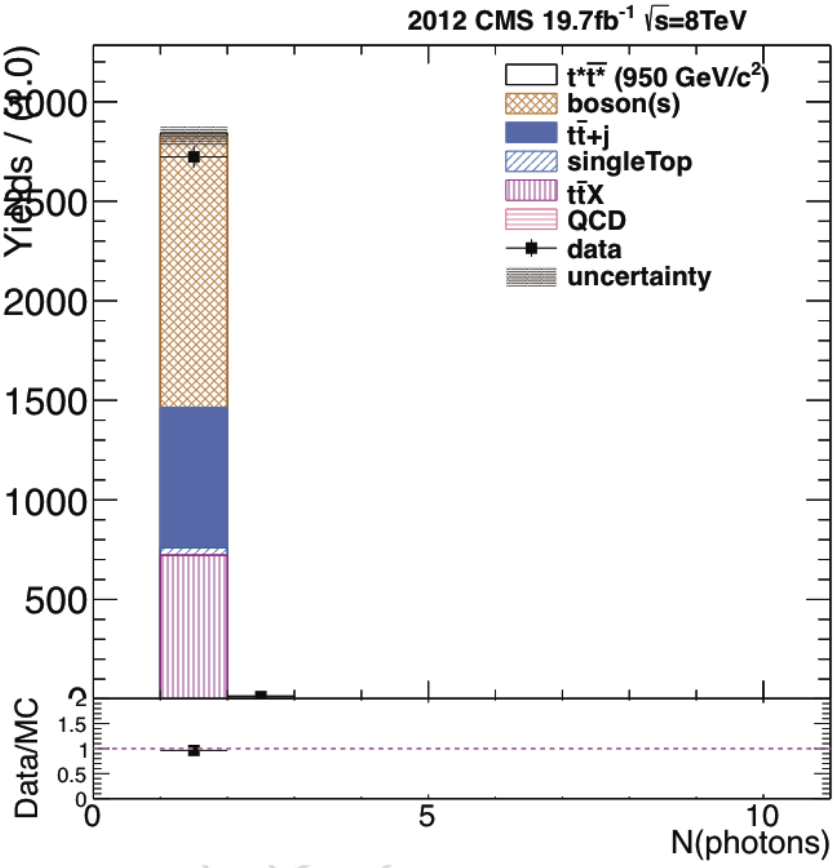

Figure 3.4: Multiplicity distribution for photon.

- Jets Reconstruction and Selections [44]: There are a lot of definition for jets it can be simply said that jets are narrow hadron cones produced by quark or gluon hadronization and showering in detector. Jet effect occurs due to quark confinement. An algorithm called anti-kt jet clustering algorithm [45] is generally used for reconstructing original parton (gluon or quark) in CMS. This algorithm is used to measure distance (d_{ij}) between two particles with the Formula 3.1 where k_{ti} is ith particle transverse momenta, $\Delta_{ij}^2 = (y_i - y_j)^2 + (\phi_i - \phi_j)^2$, ρ is a parameter to modify the relative power of the energy versus the geometrical (Δ_{ij}) scales, and R is the radius parameter. On the other hand, the distance between ith particle and beam is defined as $d_{iB} = k_{ti}^{2\rho}$. Among three different algorithm anti-kt is the one with ρ=1. Usually in CMS, cone size is taken as R=0.5.

$$d_{ij} = min(k_{ti}^{2\rho}, k_{tj}^{2\rho}) \frac{\Delta_{ij}^2}{R^2} \tag{3.1}$$

  In this analysis, jets have P_T at least 25 GeV/c and $|\eta|$<2.5. Jets, additionally, are required to pass PFjetID, this yields; neutral hadron fraction <0.99, neutral electromagnetic fraction < 0.99, number of constituents >1. Moreover, as in the photon and lepton case, a simple cleaning cut is applied (ΔR(jets,leptons)>0.5 and ΔR(jets,photons)>0.5). Multiplicity distribution for jets is given in Figure 3.5.

- Pile-up reweighting and scale factors [46]: Definition of Pile-up is dealing with multiple proton proton collisions in the same brunch crossing. There are three types of pile-up treatment depending on their time of entry in calorimeter system: in-time, out of time (late), out of time (early). In this analysis, in-time and out of time pile-ups for each bunch crossing are chosen from a Poisson distribution having a mean equal to the number of true interactions. MC samples are reweighted by using the true distributions from data and MC.

- Event selection: As in Figure 3.1, $t^*\bar{t}^* \rightarrow Wb W\bar{b}\ \gamma\gamma$. A heavy quark ($t^*$) decays $t + \gamma$ with a 100% percent branching ratio in semi-leptonic channel. On one side W decays leptonically where the charged lepton can

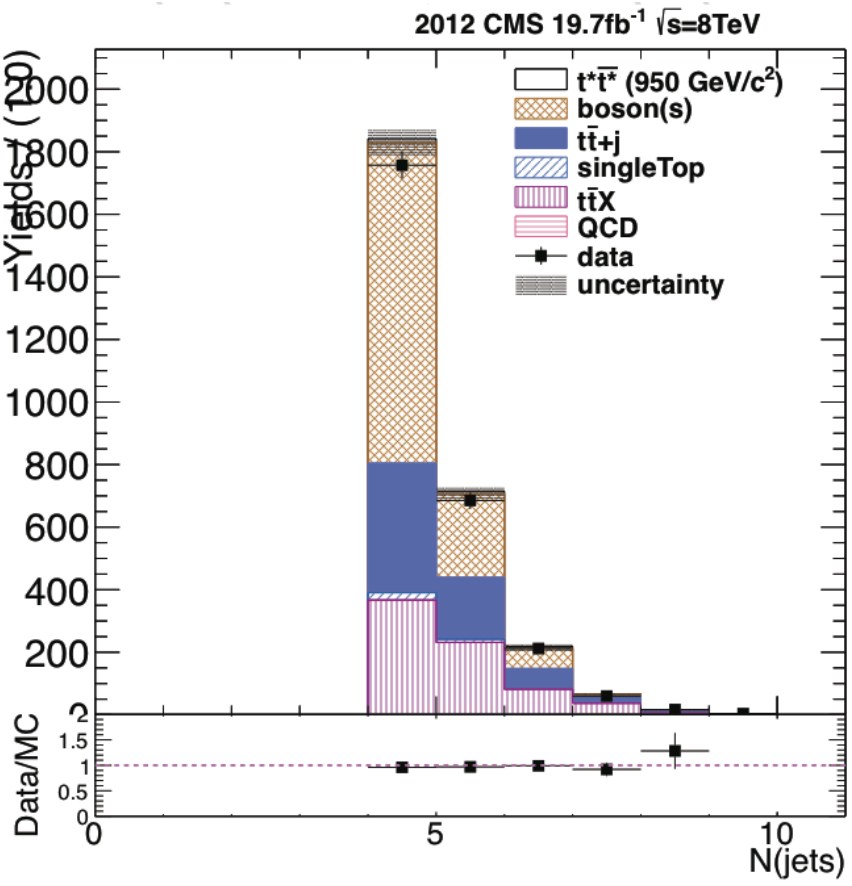

Figure 3.5: Multiplicity distribution for jets.

be either muon or electron, while on the other side W decays into 2 quarks. Therefore, selected events have exactly one electron or muon, one photon and at least 4 jets (2 from hadronic decay of W and 2 from b jets). All particles have to pass selection criteria explained before in this Section.

3.2.2 χ^2 Sorting Method

A χ^2 sorting method is implemented to reconstruct mass of t^* within events passing selection criteria in previous Section 3.2.1. This method implies to choose events have minimum χ^2 when all combination of objects' reconstruntions are in consideration. Definition of the χ^2 is given in the Formula 3.2 where W_{jj} consists of 2 jets while $W_{l\nu}$ includes a lepton and a neutrino, $t_{w_{jj}+b}(t_{w_{l\nu}+b})$ is composed of $W_{jj}(W_{l\nu})$ plus a b-jet, t* is the signal mass.

$$\chi^2 = \frac{|M_{w_{jj}} - M_W|^2}{\sigma(W_{jj})^2} + \frac{|M_{t_{w_{jj}+b}} - M_{top}|^2}{\sigma(t_{w_{jj}+b})^2} + \frac{|M_{t_{w_{l\nu}+b}} - M_{top}|^2}{\sigma(t_{w_{l\nu}+b})^2} + \frac{|t^*(t_{w_{l\nu}+b} + \gamma) - t^*(t_{w_{jj}+b} + \gamma)|^2}{\sigma(t^*_{lep})^2 + \sigma(t^*_{had})^2} \quad (3.2)$$

In the Formula 3.2, M refers to an object mass and σ indicates corresponding mass resolutions which are obtained by using MC truth information as in the Table 3.2. Moreover, objects' masses are chosen as following according to PDG values: M_W is 80.398 GeV/c^2, and M_{top} is 172.9 GeV/c^2. Since t^* mass is the one being searched, only mass difference of t^*s coming from two sides (leptonic and hadronic) is considered when calculating χ^2 .

Table3.2: Mass resolutions which are obtained by using MC truth information

	Mass Resolutions
$\sigma(W_{jj})$	9.296 GeV/c^2
$\sigma(t_{w_{jj}+b})$	16.49 GeV/c^2
$\sigma(t_{w_{l\nu}+b})$	22.43 GeV/c^2
$\sigma(t^*_{lep})$	31.63 GeV/c^2
$\sigma(t^*_{had})$	31.59 GeV/c^2

Since the transverse momenta of neutrino can be obtained from the missing transverse momenta in the experiment and since there is no machine on beam axis(z-axis), the longitudinal component of neutrino momentum needs to be calculated using a W boson mass constraint (Equation 3.3). In this analysis, solution with the minimum χ^2 is considered among two neutrino p_Z solutions coming from W boson mass constraint calculation. In Equation 3.3 W boson mass is already known and lepton for momentum can be calculated easily from detector information.

$$P_W^2 = M_W^2 = (P_\nu + P_l)^2 = P_\nu^2 + P_l^2 + 2P_\nu P_l \quad (3.3)$$

MC study of the signal reconstruction is performed by scanning the invariant mass interval between 650 GeV/c^2 and 1000 GeV/c^2 one by one for each 50

GeV/c^2 mass step. Results for assuming that there is a signal at 800 GeV/c^2 are shown in Figures 3.6, 3.7, 3.8, 3.9, 3.10, 3.11 respectively for each element of the $t^* \to t + \gamma$.

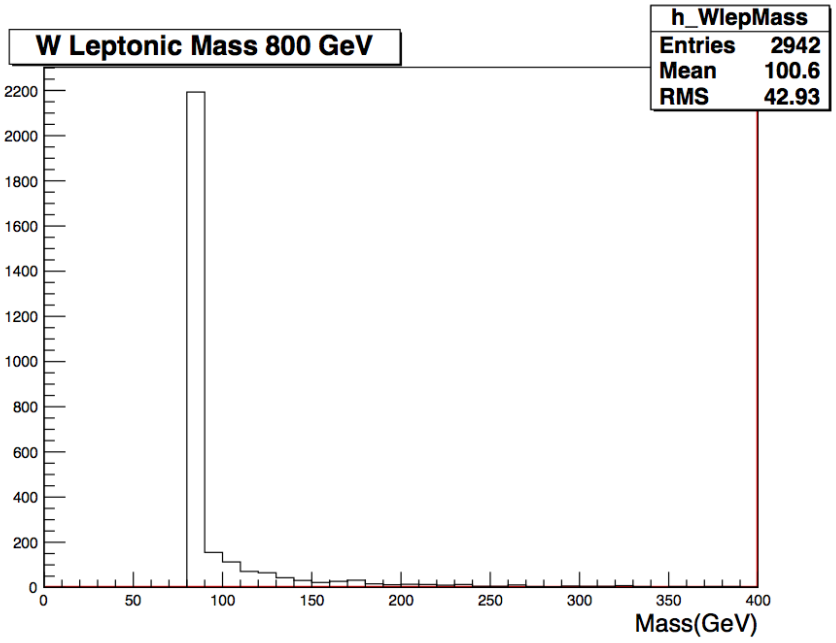

Figure 3.6: Invariant mass distribution of leptonic W boson assuming there is a signal at 800 GeV/c^2.

3.3 Fake rate calculation and Background estimation

The Matrix Method is originally used to determine isolation efficiency of lepton to estimate high-purity QCD multi-jet background from data from a low missing transverse energy signal region in $D\emptyset$ experiment at Fermilab.

Nowadays, the so called matrix method is in use for signatures which have two leptons in the final state. Generally matrix method is based on to solve linear system of equations consists of the background and signal components (unknowns), the yields three levels of selection (knowns) and coefficients of object fake rates and signal efficiencies. The three selection mentioned here stand for loose, medium and tight selection criteria.

This section is dedicated to explain adaption of the matrix method to CMS and

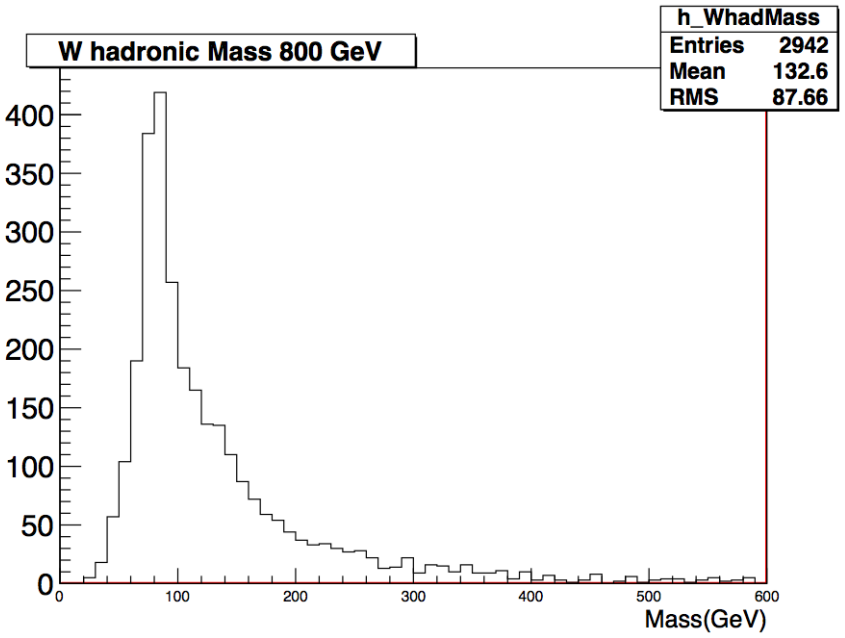

Figure 3.7: Invariant mass distribution of hadronic W boson assuming there is a signal at 800 GeV/c^2.

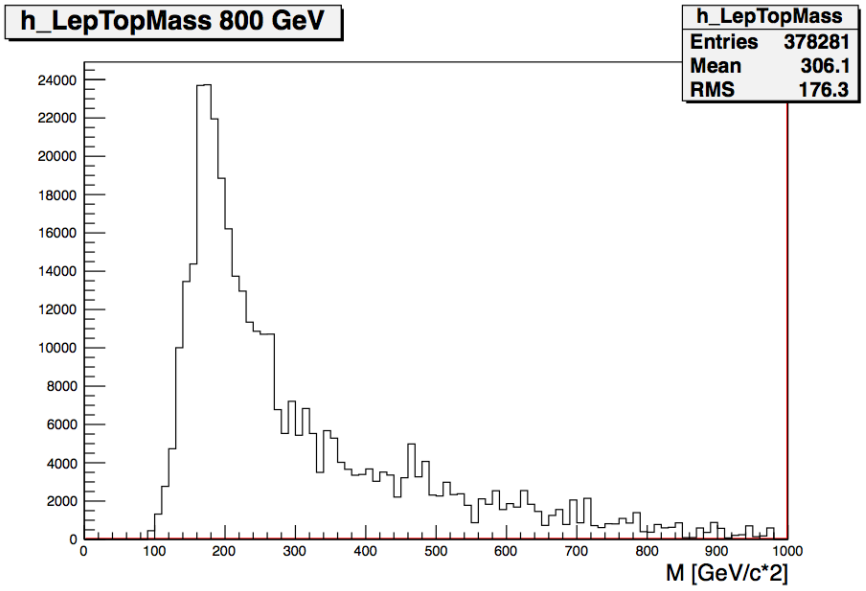

Figure 3.8: Invariant mass distribution of leptonic top quark assuming there is a signal at 800 GeV/c^2.

di-photon channel by showing detailed calculations of fake rates, efficiencies and their usage.

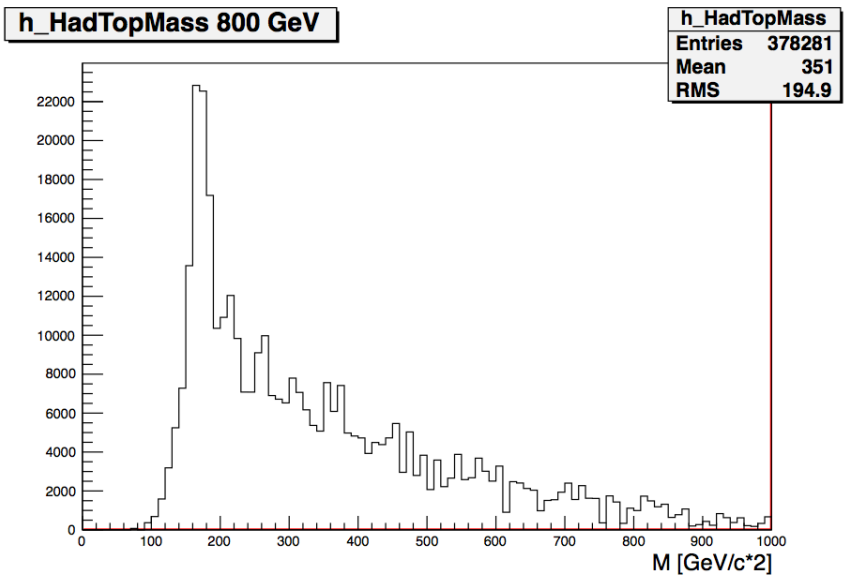

Figure 3.9: Invariant mass distribution of hadronic top quark assuming there is a signal at 800 GeV/c^2.

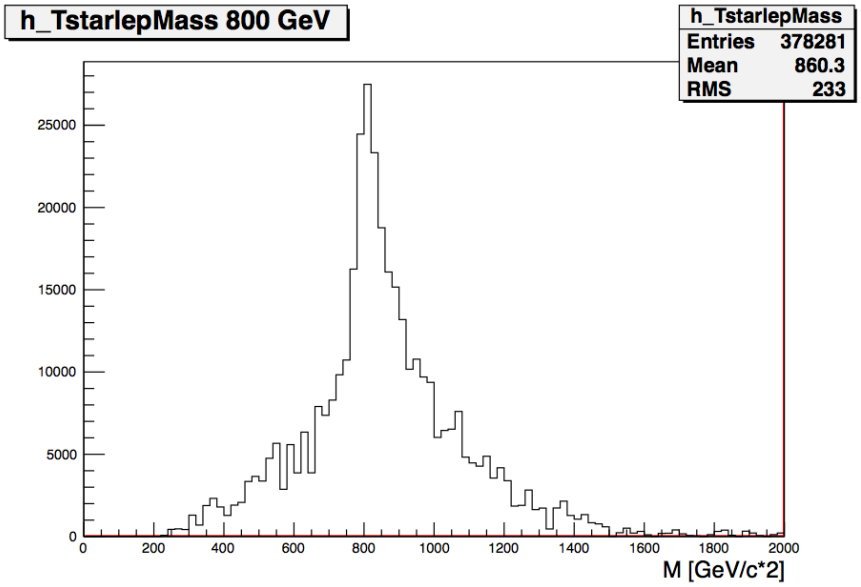

Figure 3.10: Invariant mass distribution of leptonic t^* assuming there is a signal at 800 GeV/c^2.

3.3.1 Matrix Method for Di-photon Channel

In this analysis, matrix method for di-photon channel cannot be simply applied because there are three sources of fake photons: fake photons from quarks, from gluons and fake photons from leptons. In total as matrix elements there are

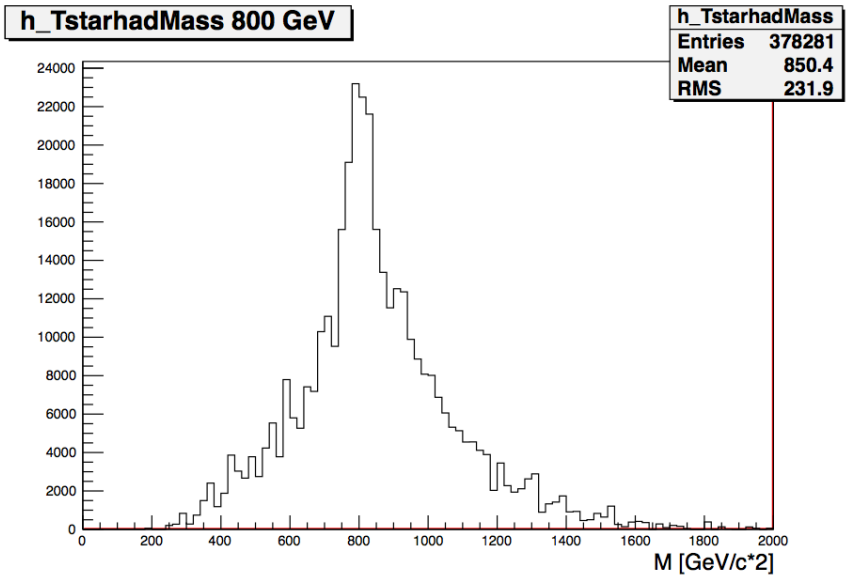

Figure 3.11: Invariant mass distribution of hadronic t^* assuming there is a signal at 800 GeV/c^2.

two photons can be both fake, both real, or one fake one real applied loose, medium, tight selections. Thus, the linear system of equation (the matrix) with 18 element can be expressed as;

$$\begin{aligned} N_L &= \left(N_L^{lq} + N_L^{lg} + N_L^{ll} + N_L^{qq} + N_L^{gg} + N_L^{qg}\right) \\ &\quad + \left(N_L^{sq} + N_L^{sg} + N_L^{sl}\right) + N_L^{ss} \qquad (3.4) \\ N_M &= \left(N_M^{lq} + N_M^{lg} + N_M^{ll} + N_M^{qq} + N_M^{gg} + N_M^{qg}\right) \\ &\quad + \left(N_M^{sq} + N_M^{sg} + N_M^{sl}\right) + N_M^{ss} \qquad (3.5) \\ N_T &= \left(N_T^{lq} + N_T^{lg} + N_T^{ll} + N_T^{qq} + N_T^{gg} + N_T^{qg}\right) \\ &\quad + \left(N_T^{sq} + N_T^{sg} + N_T^{sl}\right) + N_T^{ss} \qquad (3.6) \end{aligned}$$

In these equations, l indicates the fake photons from leptons, q and g indicates the fake photons from quarks and gluons, respectively, and s stands for the real (signal) photons. Therefore for instance N_M^{lq} will be the number of events selected by the medium isolation which have one fake photon from lepton and one fake photon from quark in the final state, while N_T^{sg} will be the number of tightly selected events with one real and one fake from gluon final state photon.

These equations can be categorized with respect to be fake or real and selected as loose, medium, tight. The definitions of yield after this catogarization are given as;

$$\begin{aligned} N^{ff}_{L(M)(T)} &\equiv N^{lq}_{L(M)(T)} + N^{lg}_{L(M)(T)} + N^{ll}_{L(M)(T)} \\ &\quad + N^{qq}_{L(M)(T)} + N^{gg}_{L(M)(T)} + N^{qg}_{L(M)(T)}, \qquad (3.7) \\ N^{sf}_{L(M)(T)} &\equiv N^{sq}_{L(M)(T)} + N^{sg}_{L(M)(T)} + N^{sl}_{L(M)(T)}. \qquad (3.8) \end{aligned}$$

$$\begin{aligned} \epsilon^{L\to M(T)}_{ff} &\equiv \frac{N^{ff}_{M(T)}}{N^{ff}_{L}}, \qquad (3.9) \\ \epsilon^{L\to M(T)}_{sf} &\equiv \frac{N^{sf}_{M(T)}}{N^{sf}_{L}}, \qquad (3.10) \\ \epsilon^{L\to M(T)}_{ss} &\equiv \frac{N^{ss}_{M(T)}}{N^{ss}_{L}}. \qquad (3.11) \end{aligned}$$

Thus, when these definitions put in to equations 3.4, 3.5, 3.6, the system of equations can be rewritten as:

$$\begin{aligned} N_L &= N^{ff}_L + N^{sf}_L + N^{ss}_L, \qquad (3.12) \\ N_M &= \epsilon^{L\to M}_{ff} N^{ff}_L + \epsilon^{L\to M}_{sf} N^{sf}_L + \epsilon^{L\to M}_{ss} N^{ss}_L, \qquad (3.13) \\ N_T &= \epsilon^{L\to T}_{ff} N^{ff}_L + \epsilon^{L\to T}_{sf} N^{sf}_L + \epsilon^{L\to T}_{ss} N^{ss}_L. \qquad (3.14) \end{aligned}$$

And the components of the ϵs:

$$\begin{aligned} \epsilon^{L\to M(T)}_{lq} &\equiv \frac{N^{lq}_{M(T)}}{N^{ff}_{L}}, \qquad (3.15) \\ \epsilon^{L\to M(T)}_{lg} &\equiv \frac{N^{lg}_{M(T)}}{N^{ff}_{L}}, \qquad (3.16) \\ \epsilon^{L\to M(T)}_{ll} &\equiv \frac{N^{ll}_{M(T)}}{N^{ff}_{L}}, \qquad (3.17) \end{aligned}$$

$$\epsilon_{qq}^{L\to M(T)} \equiv \frac{N_{M(T)}^{qq}}{N_L^{ff}}, \tag{3.18}$$

$$\epsilon_{gg}^{L\to M(T)} \equiv \frac{N_{M(T)}^{gg}}{N_L^{ff}}, \tag{3.19}$$

$$\epsilon_{qg}^{L\to M(T)} \equiv \frac{N_{M(T)}^{qg}}{N_L^{ff}}, \tag{3.20}$$

$$\epsilon_{sq}^{L\to M(T)} \equiv \frac{N_{M(T)}^{sq}}{N_L^{sf}}, \tag{3.21}$$

$$\epsilon_{sg}^{L\to M(T)} \equiv \frac{N_{M(T)}^{sg}}{N_L^{sf}}, \tag{3.22}$$

$$\epsilon_{sl}^{L\to M(T)} \equiv \frac{N_{M(T)}^{sl}}{N_L^{sf}}. \tag{3.23}$$

Since ϵs are linearly independent coefficients can be written:

$$\begin{aligned}\epsilon_{ff}^{L\to M(T)} &= \epsilon_{lq}^{L\to M(T)} + \epsilon_{lg}^{L\to M(T)} + \epsilon_{ll}^{L\to M(T)} \\ &\quad + \epsilon_{qq}^{L\to M(T)} + \epsilon_{gg}^{L\to M(T)} + \epsilon_{qg}^{L\to M(T)} \qquad (3.24)\\ \epsilon_{sf}^{L\to M(T)} &= \epsilon_{sq}^{L\to M(T)} + \epsilon_{sg}^{L\to M(T)} + \epsilon_{sl}^{L\to M(T)} \qquad (3.25)\end{aligned}$$

In order to define elements can be estimated from data, the following calculations are necessary.

$$\begin{aligned}\epsilon_{lq}^{L\to T} &= \frac{N_T^{lq}}{N_L^{lq} + N_L^{lg} + N_L^{ll} + N_L^{qq} + N_L^{gg} + N_L^{qg}} \\ &= \frac{N_T^{lq}}{N_L^{lq}} \cdot \frac{1}{1 + \frac{N_L^{lg}}{N_L^{lq}} + \frac{N_L^{ll}}{N_L^{lq}} + \frac{N_L^{qq}}{N_L^{lq}} + \frac{N_L^{gg}}{N_L^{lq}} + \frac{N_L^{qg}}{N_L^{lq}}} \\ &= \epsilon_l\epsilon_q \cdot \frac{1}{1 + R^{lg/lq} + R^{ll/lq} + R^{qq/lq} + R^{gg/lq} + R^{qg/lq}} \\ \epsilon_{lg}^{L\to T} &= \frac{N_T^{lg}}{N_L^{lq} + N_L^{lg} + N_L^{ll} + N_L^{qq} + N_L^{gg} + N_L^{qg}} \\ &= \frac{N_T^{lg}}{N_L^{lg}} \cdot \frac{1}{1 + \frac{N_L^{lq}}{N_L^{lg}} + \frac{N_L^{ll}}{N_L^{lg}} + \frac{N_L^{qq}}{N_L^{lg}} + \frac{N_L^{gg}}{N_L^{lg}} + \frac{N_L^{qg}}{N_L^{lg}}} \\ &= \epsilon_l\epsilon_g \cdot \frac{1}{1 + R^{lq/lg} + R^{ll/lg} + R^{qq/lg} + R^{gg/lg} + R^{qg/lg}}\end{aligned}$$

$$
\begin{aligned}
\epsilon_{ll}^{L\to T} &= \frac{N_T^{ll}}{N_L^{lq}+N_L^{lg}+N_L^{ll}+N_L^{qq}+N_L^{gg}+N_L^{qg}} \\
&= \frac{N_T^{ll}}{N_L^{ll}}\cdot\frac{1}{1+\frac{N_L^{lq}}{N_L^{ll}}+\frac{N_L^{lg}}{N_L^{ll}}+\frac{N_L^{qq}}{N_L^{ll}}+\frac{N_L^{gg}}{N_L^{ll}}+\frac{N_L^{qg}}{N_L^{ll}}} \\
&= \epsilon_l^2\cdot\frac{1}{1+R^{lq/ll}+R^{lg/ll}+R^{qq/ll}+R^{gg/ll}+R^{qg/ll}}, \\
\epsilon_{qq}^{L\to T} &= \frac{N_T^{qq}}{N_L^{lq}+N_L^{lg}+N_L^{ll}+N_L^{qq}+N_L^{gg}+N_L^{qg}} \\
&= \frac{N_T^{qq}}{N_L^{qq}}\cdot\frac{1}{1+\frac{N_L^{lq}}{N_L^{qq}}+\frac{N_L^{lg}}{N_L^{qq}}+\frac{N_L^{ll}}{N_L^{qq}}+\frac{N_L^{gg}}{N_L^{qq}}+\frac{N_L^{qg}}{N_L^{qq}}} \\
&= \epsilon_q^2\cdot\frac{1}{1+R^{lq/qq}+R^{lg/qq}+R^{ll/qq}+R^{gg/qq}+R^{qg/qq}} \\
\epsilon_{gg}^{L\to T} &= \frac{N_T^{gg}}{N_L^{lq}+N_L^{lg}+N_L^{ll}+N_L^{qq}+N_L^{gg}+N_L^{qg}} \\
&= \frac{N_T^{gg}}{N_L^{gg}}\cdot\frac{1}{1+\frac{N_L^{lq}}{N_L^{gg}}+\frac{N_L^{lg}}{N_L^{gg}}+\frac{N_L^{ll}}{N_L^{gg}}+\frac{N_L^{qq}}{N_L^{gg}}+\frac{N_L^{qg}}{N_L^{gg}}} \\
&= \epsilon_g^2\cdot\frac{1}{1+R^{lq/gg}+R^{lg/gg}+R^{ll/gg}+R^{qq/gg}+R^{qg/gg}} \\
\epsilon_{qg}^{L\to T} &= \frac{N_T^{qg}}{N_L^{lq}+N_L^{lg}+N_L^{ll}+N_L^{qq}+N_L^{gg}+N_L^{qg}} \\
&= \frac{N_T^{qg}}{N_L^{qg}}\cdot\frac{1}{1+\frac{N_L^{lq}}{N_L^{qg}}+\frac{N_L^{lg}}{N_L^{qg}}+\frac{N_L^{ll}}{N_L^{qg}}+\frac{N_L^{qq}}{N_L^{qg}}+\frac{N_L^{gg}}{N_L^{qg}}} \\
&= \epsilon_q\epsilon_g\cdot\frac{1}{1+R^{lq/qg}+R^{lg/qg}+R^{ll/qg}+R^{qq/qg}+R^{gg/qg}}
\end{aligned}
$$

$$
\begin{aligned}
\epsilon_{lq}^{L\to M} &= \frac{N_M^{lq}}{N_L^{lq}+N_L^{lg}+N_L^{ll}+N_L^{qq}+N_L^{gg}+N_L^{qg}} \\
&= \frac{N_M^{lq}}{N_L^{lq}}\cdot\frac{1}{1+\frac{N_L^{lg}}{N_L^{lq}}+\frac{N_L^{ll}}{N_L^{lq}}+\frac{N_L^{qq}}{N_L^{lq}}+\frac{N_L^{gg}}{N_L^{lq}}+\frac{N_L^{qg}}{N_L^{lq}}} \\
&= (\epsilon_l+\epsilon_q-\epsilon_l\epsilon_q)\cdot\frac{1}{1+R^{lg/lq}+R^{ll/lq}+R^{qq/lq}+R^{gg/lq}+R^{qg/lq}} \\
\epsilon_{lg}^{L\to M} &= \frac{N_M^{lg}}{N_L^{lq}+N_L^{lg}+N_L^{ll}+N_L^{qq}+N_L^{gg}+N_L^{qg}} \\
&= \frac{N_M^{lg}}{N_L^{lg}}\cdot\frac{1}{1+\frac{N_L^{lq}}{N_L^{lg}}+\frac{N_L^{ll}}{N_L^{lg}}+\frac{N_L^{qq}}{N_L^{lg}}+\frac{N_L^{gg}}{N_L^{lg}}+\frac{N_L^{qg}}{N_L^{lg}}} \\
&= (\epsilon_l+\epsilon_g-\epsilon_l\epsilon_g)\cdot\frac{1}{1+R^{lq/lg}+R^{ll/lg}+R^{qq/lg}+R^{gg/lg}+R^{qg/lg}}
\end{aligned}
$$

$$
\begin{aligned}
\epsilon_{ll}^{L\to M} &= \frac{N_M^{ll}}{N_L^{lq}+N_L^{lg}+N_L^{ll}+N_L^{qq}+N_L^{gg}+N_L^{qg}} \\
&= \frac{N_M^{ll}}{N_L^{ll}}\cdot\frac{1}{1+\frac{N_L^{lq}}{N_L^{ll}}+\frac{N_L^{lg}}{N_L^{ll}}+\frac{N_L^{qq}}{N_L^{ll}}+\frac{N_L^{gg}}{N_L^{ll}}+\frac{N_L^{qg}}{N_L^{ll}}} \\
&= \left(2\epsilon_l-\epsilon_l^2\right)\cdot\frac{1}{1+R^{lq/ll}+R^{lg/ll}+R^{qq/ll}+R^{gg/ll}+R^{qg/ll}} \\
\epsilon_{qq}^{L\to M} &= \frac{N_M^{qq}}{N_L^{lq}+N_L^{lg}+N_L^{ll}+N_L^{qq}+N_L^{gg}+N_L^{qg}} \\
&= \frac{N_M^{qq}}{N_L^{qq}}\cdot\frac{1}{1+\frac{N_L^{lq}}{N_L^{qq}}+\frac{N_L^{lg}}{N_L^{qq}}+\frac{N_L^{ll}}{N_L^{qq}}+\frac{N_L^{gg}}{N_L^{qq}}+\frac{N_L^{qg}}{N_L^{qq}}} \\
&= \left(2\epsilon_q-\epsilon_q^2\right)\cdot\frac{1}{1+R^{lq/qq}+R^{lg/qq}+R^{ll/qq}+R^{gg/qq}+R^{qg/qq}} \\
\epsilon_{gg}^{L\to M} &= \frac{N_M^{gg}}{N_L^{lq}+N_L^{lg}+N_L^{ll}+N_L^{qq}+N_L^{gg}+N_L^{qg}} \\
&= \frac{N_M^{gg}}{N_L^{gg}}\cdot\frac{1}{1+\frac{N_L^{lq}}{N_L^{gg}}+\frac{N_L^{lg}}{N_L^{gg}}+\frac{N_L^{ll}}{N_L^{gg}}+\frac{N_L^{qq}}{N_L^{gg}}+\frac{N_L^{qg}}{N_L^{gg}}} \\
&= \left(2\epsilon_g-\epsilon_g^2\right)\cdot\frac{1}{1+R^{lq/gg}+R^{lg/gg}+R^{ll/gg}+R^{qq/gg}+R^{qg/gg}} \\
\epsilon_{qg}^{L\to M} &= \frac{N_M^{qg}}{N_L^{lq}+N_L^{lg}+N_L^{ll}+N_L^{qq}+N_L^{gg}+N_L^{qg}} \\
&= \frac{N_M^{qg}}{N_L^{qg}}\cdot\frac{1}{1+\frac{N_L^{lq}}{N_L^{qg}}+\frac{N_L^{lg}}{N_L^{qg}}+\frac{N_L^{ll}}{N_L^{qg}}+\frac{N_L^{qq}}{N_L^{qg}}+\frac{N_L^{gg}}{N_L^{qg}}} \\
&= (\epsilon_q+\epsilon_g-\epsilon_q\epsilon_g)\cdot\frac{1}{1+R^{lq/qg}+R^{lg/qg}+R^{ll/qg}+R^{qq/qg}+R^{gg/qg}}
\end{aligned}
$$

$$
\begin{aligned}
\epsilon_{sq}^{L\to T} &= \frac{N_T^{sq}}{N_L^{sq}+N_L^{sg}+N_L^{sl}} = \frac{N_T^{sq}}{N_L^{sq}}\cdot\frac{1}{1+\frac{N_L^{sg}}{N_L^{sq}}+\frac{N_L^{sl}}{N_L^{sq}}} \\
&= \epsilon_s\epsilon_q\cdot\frac{1}{1+R^{sg/sq}+R^{sl/sq}}, \\
\epsilon_{sg}^{L\to T} &= \frac{N_T^{sg}}{N_L^{sq}+N_L^{sg}+N_L^{sl}} = \frac{N_T^{sg}}{N_L^{sg}}\cdot\frac{1}{1+\frac{N_L^{sq}}{N_L^{sg}}+\frac{N_L^{sl}}{N_L^{sg}}} \\
&= \epsilon_s\epsilon_g\cdot\frac{1}{1+R^{sq/sg}+R^{sl/sg}}, \\
\epsilon_{sl}^{L\to T} &= \frac{N_T^{sl}}{N_L^{sq}+N_L^{sg}+N_L^{sl}} = \frac{N_T^{sl}}{N_L^{sl}}\cdot\frac{1}{1+\frac{N_L^{sq}}{N_L^{sl}}+\frac{N_L^{sg}}{N_L^{sl}}} \\
&= \epsilon_s\epsilon_l\cdot\frac{1}{1+R^{sq/sl}+R^{sg/sl}},
\end{aligned}
$$

$$
\begin{aligned}
\epsilon_{sq}^{L\to M} &= \frac{N_M^{sq}}{N_L^{sq}+N_L^{sg}+N_L^{sl}} = \frac{N_M^{sq}}{N_L^{sq}} \cdot \frac{1}{1+\frac{N_L^{sg}}{N_L^{sq}}+\frac{N_L^{sl}}{N_L^{sq}}} \\
&= (\epsilon_s+\epsilon_q-\epsilon_s\epsilon_q)\cdot\frac{1}{1+R^{sg/sq}+R^{sl/sq}}, \\
\epsilon_{sg}^{L\to M} &= \frac{N_M^{sg}}{N_L^{sq}+N_L^{sg}+N_L^{sl}} = \frac{N_M^{sg}}{N_L^{sg}} \cdot \frac{1}{1+\frac{N_L^{sq}}{N_L^{sg}}+\frac{N_L^{sl}}{N_L^{sg}}} \\
&= (\epsilon_s+\epsilon_g-\epsilon_s\epsilon_g)\cdot\frac{1}{1+R^{sq/sg}+R^{sl/sg}}, \\
\epsilon_{sl}^{L\to M} &= \frac{N_M^{sl}}{N_L^{sq}+N_L^{sg}+N_L^{sl}} = \frac{N_M^{sl}}{N_L^{sl}} \cdot \frac{1}{1+\frac{N_L^{sq}}{N_L^{sl}}+\frac{N_L^{sg}}{N_L^{sl}}} \\
&= (\epsilon_s+\epsilon_l-\epsilon_s\epsilon_l)\cdot\frac{1}{1+R^{sq/sl}+R^{sg/sl}}, \\
\epsilon_{ss}^{L\to T} &= \frac{N_T^{ss}}{N_L^{ss}} = \epsilon_s^2, \\
\epsilon_{ss}^{L\to M} &= \frac{N_M^{ss}}{N_L^{ss}} = 2\epsilon_s-\epsilon_s^2.
\end{aligned}
$$

where the ratio factors $R^{xy/st}$ are defined as following:

$$
R^{xy/st} \equiv \frac{N_L^{xy}}{N_L^{st}}. \tag{3.26}
$$

The system of equations can be solved by estimating the object-level efficiencies (ϵ_l, ϵ_q, ϵ_g, ϵ_s) and the ratio factors from data.

Application of this method to the t^* di-photon channel will be discussed in the following subsections.

The efficiency ϵ_l can be estimated from a Tag and Probe technique on an electron-photon sample, while the efficiency ϵ_q, ϵ_g can be estimated with a template fitting procedure on QCD enriched sample. The real photon efficiency ϵ_s can be calculated again by means of a Tag and Probe technique, by fitting the invariant mass of the di-muon gamma sample. Finally, the ratio factors are estimated by counting the number of two object events in the signal region of the samples.

The estimation of background events number containing one or two fake photons from data depends on estimation of the efficiency and ratio factors from data.

The following subsections are reserved for describing the procedure of the ratio factors, the fake rate from leptons, from jets (produced by the hadronization of quark-like and gluon-like partons), and the real photon efficiency estimations from data.

3.3.1.1 Photon Fake Rate from leptons

Initially, it should be noted that ϵs should be seen as a relative fake rate because they are defined to be a ratio of fake rates (or signal efficiencies). In the case of the fake rate from leptons, two selections are defined to calculate the ratio: tight selection, no-electron-veto selection. The tight selection is the usual tight ID photon selection, while the no-electron-veto selection will be the tight ID selection with the exception of the electron-veto cut. Thus, the ϵ_l is defined as the per-object ratio of the photon fake rate for the tight selection over the fake rate for the no-electron-veto selection.

A Tag and Probe technique, explained at the end of this subsection, is used in order to count the number of fake photons for the tight and no-electron-veto selection. Figure 3.12 shows the invariant mass of an electron and a photon fitted with a BreitWigner [47] convoluted to a Crystall Ball [47] (for the signal) with a fast Fourier transformation plus a CMSShape (for the background) where CMSShape can be defined as complementary error function multiplied with an exponential. The implementation of this function can be found in corresponding directory of CMSSW [3]. This permits to subtract the non Drell-Yan component. As in the Figure, the fit is performed in the invariant mass range between 60 and 120 GeV. The number of fake photons for ϵ_l calculation is the signal event number of these two fitted distributions.

For the object selection for fake photon calculation, electrons passed tight selections and with transverse momenta larger 20 GeV/c are investigated. The transverse momenta cut was 30 GeV/c for the mass reconstruction in Section 3.2.1, it is lowered to get enough statistics at the low end of the invariant mass distribution. Moreover, the kinematic photon selection and event selection is

[3] /CMSSW/PhysicsTools/TagAndProbe/interface

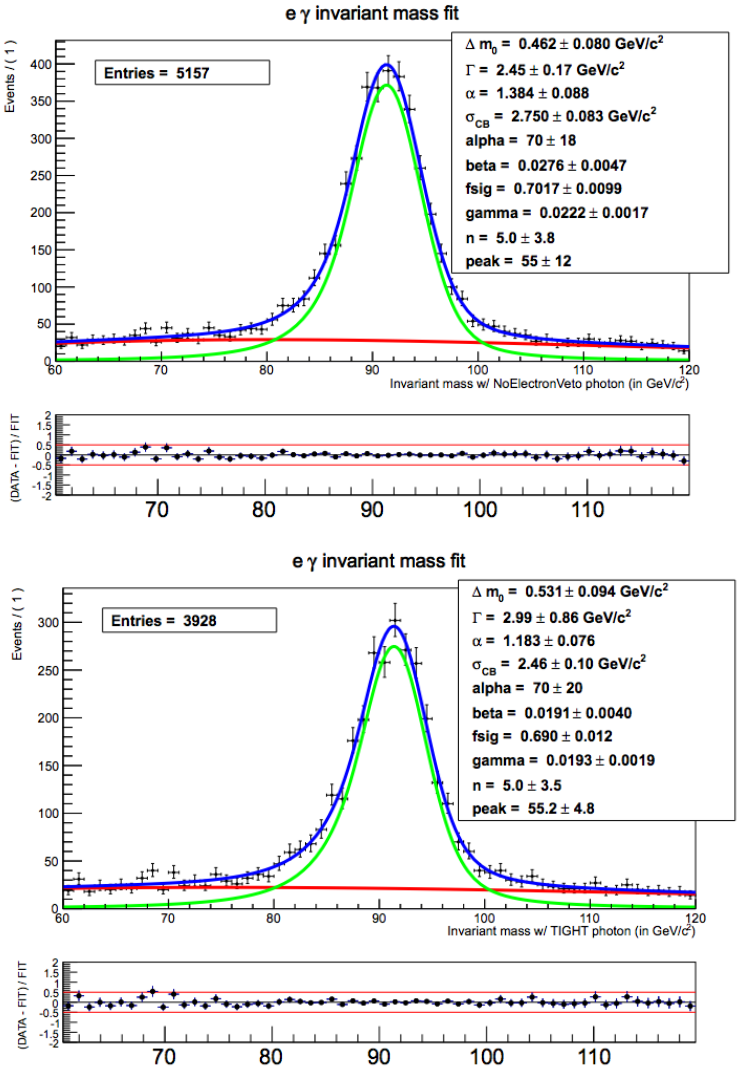

Figure 3.12: Electron-Photon invariant mass fit for the no-electron-veto selection (upper plot) and the tight ID selection (lower plot). The fit function is a BreitWigner convoluted to a Crystall Ball with a fast Fourier transformation (for the signal) plus a CMSShape (for the background).

the same as in the Section 3.2.1. η, Jet multiplicity, vertex multiplicity and transverse momentum dependencies of ϵ_l can be seen in Figures 3.13, 3.14, 3.15, 3.16.

Tag and Probe Method [48]: Efficiencies can be calculated by using tag and probe which is data driven technique. A mass resonance (i.e. J/ψ, upsilon or Z), or a well known PDF is needed for this calculation. The Tag is a muon or electron that passed from a very tight selection criteria and therefore have a very

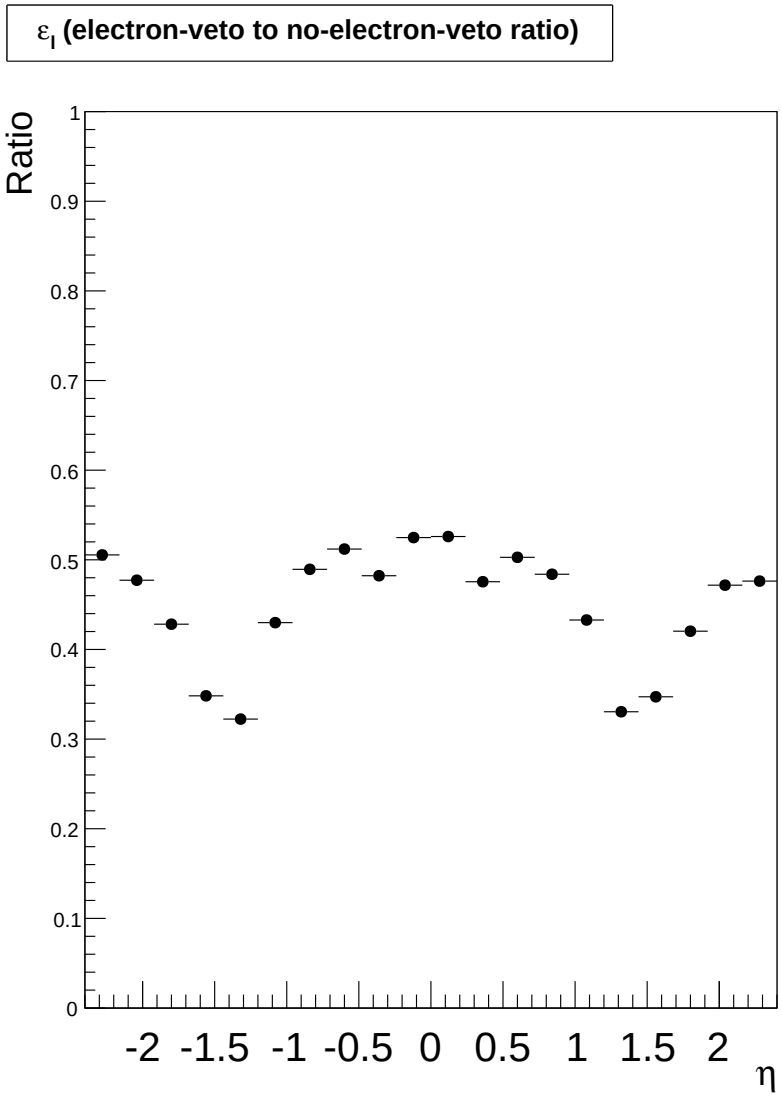

Figure 3.13: ϵl: electron-veto to no-electron-veto ratio to Eta .

low fake rate while the probe has looser criteria. Moreover, The passing Probe has tighter criteria than the Probe, but not tighter than the Tag.

3.3.1.2 Photon Fake Rate from jets

A template fitting technique is used to estimate the contribution from fake photons from jets. Defining a fakeable object is appropriate for efficiency calculation within this method. The fakeable object is defined as an EM SuperCluster (SC) has certain characteristics:

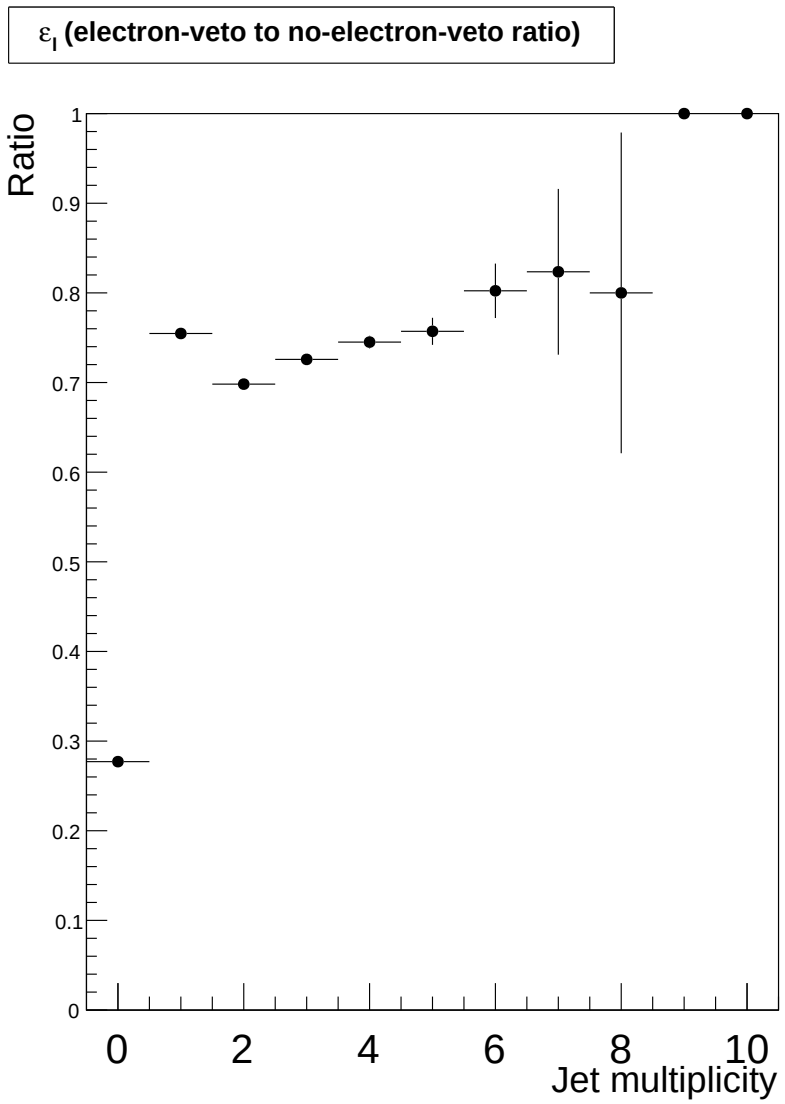

Figure 3.14: ϵl: electron-veto to no-electron-veto ratio to NJets .

- The SC has to be close to a jet within a ΔR distance of 0.5. This should reduce the real photon contamination.

- The SC has to pass looser ID cuts, with respect to the tight ID selection. The ID cuts are loosened by a factor of 5.

- The SC has to pass inverted tight ID cuts, for 1/5 of the H/E tower threshold, the charge isolation, the neutral isolation and the photon isolation cuts.

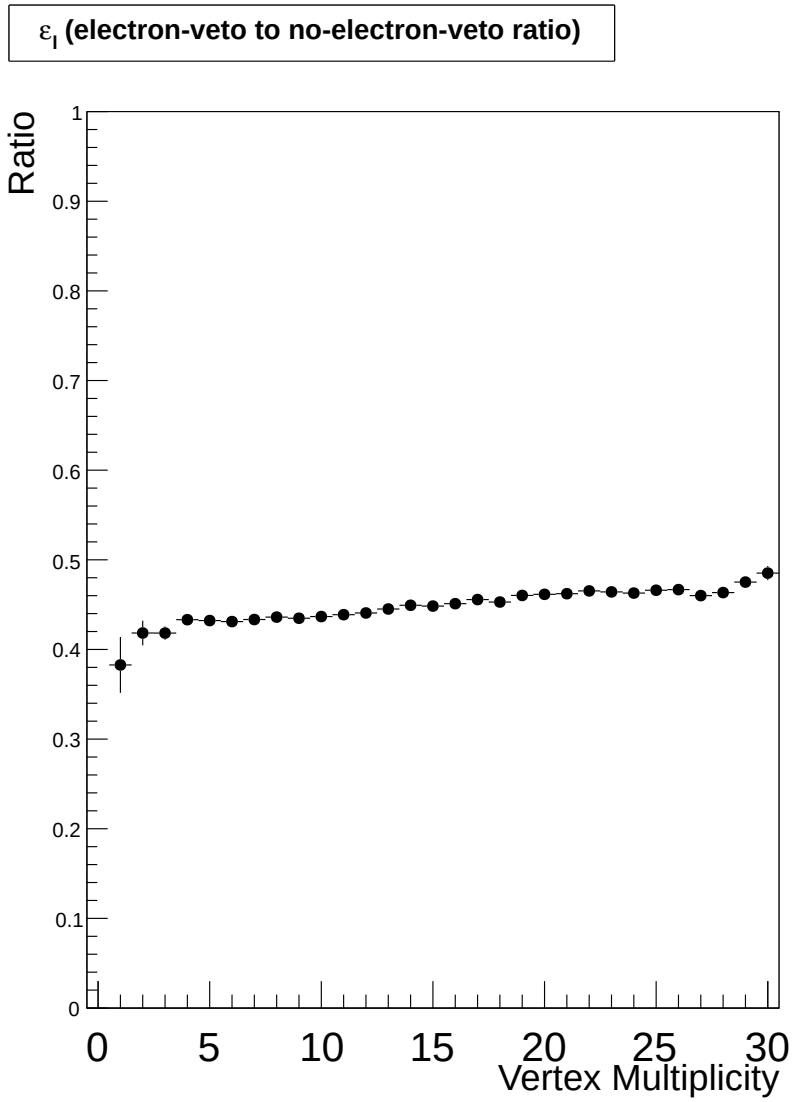

Figure 3.15: ϵl: electron-veto to no-electron-veto ratio to NVTX .

Once the FO is defined, the $\sigma_{i\eta i\eta}$ distribution of these objects can be fitted according to a template fit and obtain the signal fraction (which in this case will determine the number of fake photons from jets) and subtract the background component (which will be represented by the real photons).

In order to perform the fit, the background and signal templates are obtained respectively from data and from MC corrected with data-driven correction factors.

The corrections for the signal are the following:

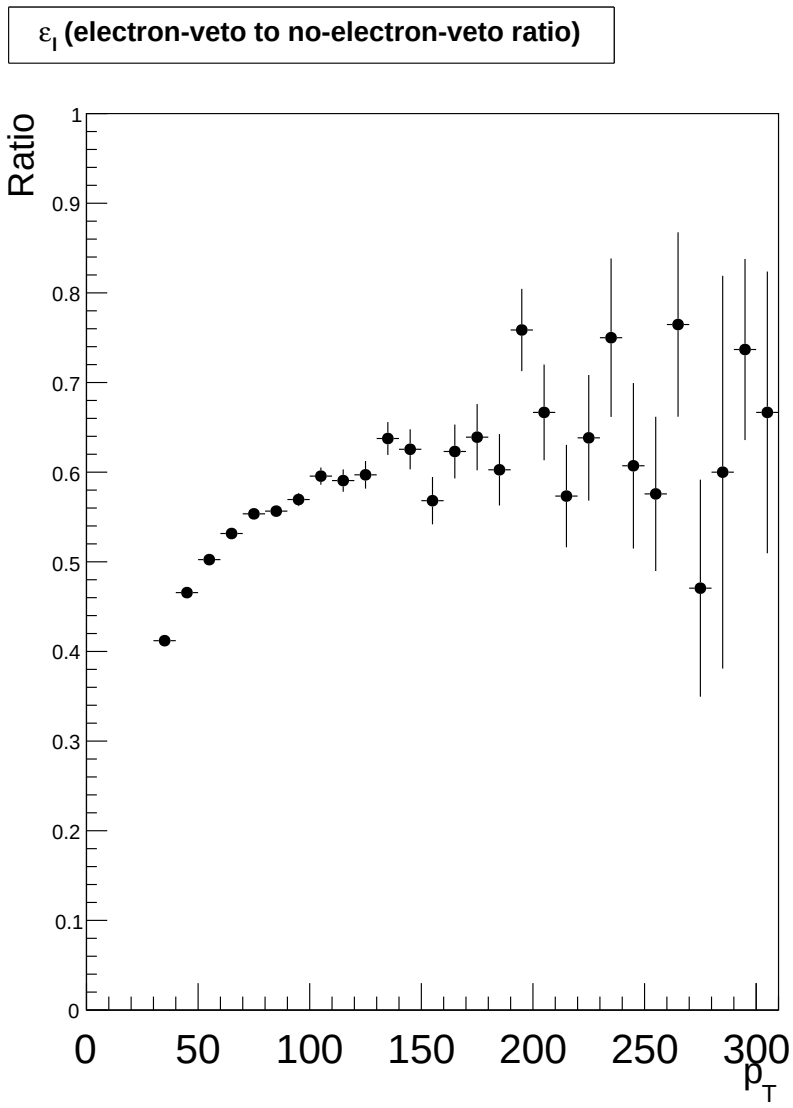

Figure 3.16: ϵl: electron-veto to no-electron-veto ratio to P_T .

$$\sigma_{i\eta i\eta}^{EBcorr} = (\sigma_{i\eta i\eta} - 0.0090405) \times 1.04 + 0.0089405$$
$$\sigma_{i\eta i\eta}^{EEcorr} = \sigma_{i\eta i\eta} \times 1.1 - 0.0025 \tag{3.27}$$

In Eq. 3.27 , $\sigma_{i\eta i\eta}^{EBcorr}$ is for the Barrel and $\sigma_{i\eta i\eta}^{EEcorr}$ is for Endcap photons. Furthermore, the possible residual small differences between the true signal shapes and those used in the fit are taken into account by applying a systematic uncertainty on the shape while calculating the ϵ_js.

The MC process used to infer the signal templates is the photon+jets, which has transverse momentum spectra reasonably similar to that of the all background processes.

The background templates are taken directly from the data. The FO definition has been optimized to obtain a signal photon contamination fraction of less than 1%. In addition to this it is verified that the background $\sigma_{i\eta i\eta}$ shape for the FO definition and the tight ID definition are reasonably similar using the MC. However, any possible residual difference is taken into account from the shape systematic.

After the shapes are obtained the Barrel and Endcap $\sigma_{i\eta i\eta}$ distribution separately can be fitted. The fit is performed on the entire $\sigma_{i\eta i\eta}$ range, but it is integrated over the tight ID $\sigma_{i\eta i\eta}$ range to obtain the number of events and the signal fraction.

The results for photon fake rate from jets will be represented as CMS Physics analysis note [49]. The final results for fake rate calculations are given in Section 3.3.1.5.

3.3.1.3 Photon Signal Efficiency

In this case again a Tag and Probe technique is used as in the case of the fake rate from leptons. The ϵ_s is defined the per-object ratio of the photon efficiency for the tight selection over the sum of the efficiencies for the no-electron-veto selection and the FO selection. However, the FO selection has been optimized to have negligible real photon contamination, therefore it will not be taken into account.

In order to count the number of fake photons for the tight and no-electron-veto selection, Tag and Probe technique is applied on the invariant mass of the muon-muon-photon system.

For the fit of the invariant mass a BreitWigner convoluted to a Gaussian (for the signal) with a fast Fourier transformation plus a CMSShape for the Background.

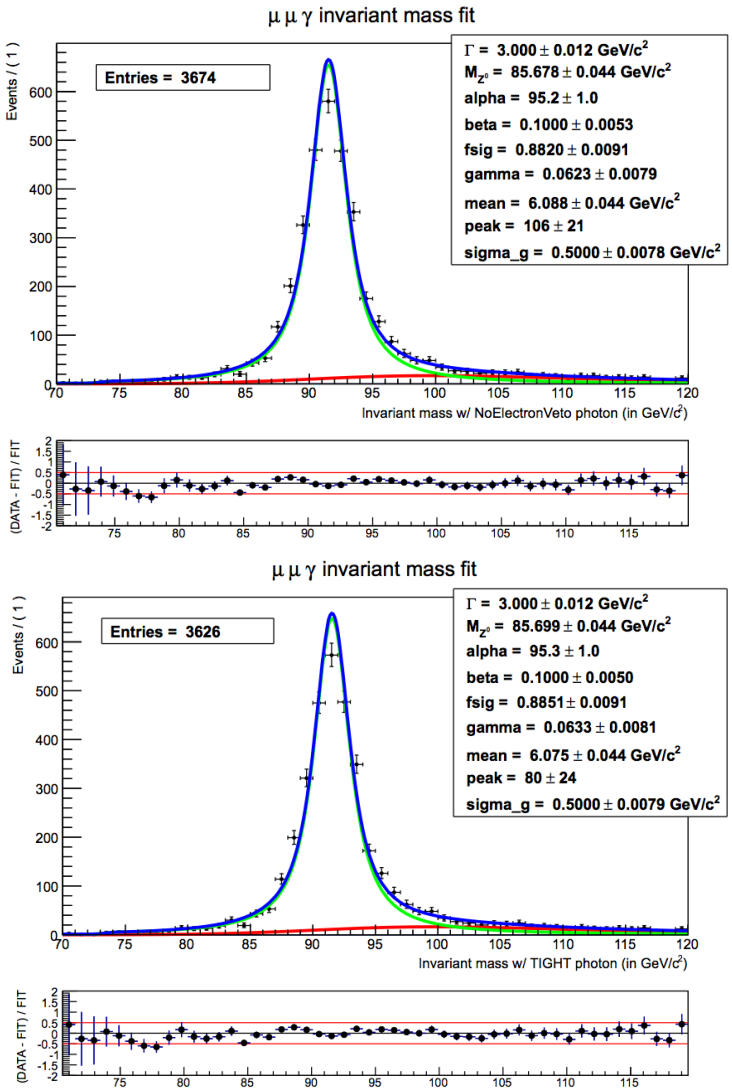

Figure 3.17: Muon-Muon-Photon invariant mass fit for the no-electron-veto selection (upper plot) and the tight ID selection (lower plot). The fit function is a BreitWigner convoluted thanks to a fast Fourier transformation to a Gaussian (for the signal) plus a CMSShape (for the background).

This allows to subtract the non Drell-Yan component. The final number of fitted signal events is the number of real photons to be used for the ϵ_s calculation.

For the object selection for fake photon calculation, it is observed that the jet multiplicity has no effect on this calculation so no selection on the jet multiplicity is applied for the photon signal efficiency calculation. The transverse momentum of the photon is larger then 30 GeV/c. On the leading muon transverse momentum we apply a tight selection and we lower the transverse momenta cri-

teria to 20 GeV in order to get enough statistics at the low end of the invariant mass distribution.

Figure 3.17 shows the fit performed in the invariant mass range between 70 and 120 GeV. Both DoubleMu and SingleMu Primary Datasets are used to increase statistics.

3.3.1.4 Ratio Factors

The ratio factors are determined from the data. To determined all the ratio factors is enough to determine the following number of events: N_L^{sl}, N_L^{sq}, N_L^{sg}, N_L^{qg}, N_L^{lg}, N_L^{lq}, N_L^{ll}, N_L^{qq}, N_L^{gg}.

In a good approximation the above number of events can be obtained by selecting two photons events in which s, l, g, q photons can be requested as a tight, anti-electron-veto, FO Quark-like and FO Gluon-like object, respectively. Any contamination due to this approximation can be subtracted from MC the non-matching component (where in this case the matching is a MC matching to obtain true objects).

Given the FO definition used the number of two photon-like object events containing at least one FO is small. In order to increase the statistics another FO definition has been used. The alternative FO definition has been used to infer the ratio factors, after applying a correction factor which is derived from the data. The correction factor takes into account the ratio of the two FO definitions on a per-object base.

3.3.1.5 Results of Fake Rate Calculations

The N_T^{ff} and N_T^{sf} can be obtained by matrix inversion after the ratio factors, real photon efficiency and the fake rates are calculated. 10 Million pseudo-experiments are used in order to calculate the uncertainties. In the pseudo-experiments the ratio factors and the ϵs are allowed to alter within their uncertainties.

The final results are: $N_{sf}^{T} = 7.9 \pm 0.4$ and $N_{ff}^{T} = 1.7 \pm 0.08$.

CHAPTER 4

CONCLUSION

Pair produced excited quark, t^*, which decays exclusively to a top quark and a photon, is investigated by considering semi-leptonic decay channel. In final state, there are two isolated photons, at least 4 well-reconstructed jets and one lepton, which can be either a single isolated muon or electron. Furthermore, the χ^2 sorting method and matrix method is presented to reconstruct signal and to determine fake rate of photons coming from leptons and jets, respectively. Tag and Probe method and QCD-enriched samples are also implied to make use of matrix method. Tag and Probe method is used to calculate fake rates from leptons and real photon efficiency while QCD-enriched samples with likelihood fitting are used to calculate fake rate from jets. As shown in Section 3.3.1.5, number of events with two photons passing tight selection for one fake and one real case (N_{sf}^T) is 7.9 ± 0.4 while for two fake photon case (N_{ff}^T) is 1.7 ± 0.08. These results are obtained by inverting the matrix given by the linear equation system combined of three equations 3.4, 3.5, 3.6. Moreover, electron-photon sample is used to obtain Z boson mass distribution used for fake rate from leptons calculations. On the other hand, muon-muon-photon samples are used for calculating real photon efficiency. In addition, results for fake rate from jets will be represented as CMS Physics analysis note [49]. In this study, proton-proton collision data collected by CMS at 8 TeV corresponding to an integrated luminosity of $19.6 fb^{-1}$ is investigated. Luminosity is number of events (N) in a certain time t. Thus, the integrated luminosity is the time integral of the luminosity. Analysis is performed in a model independent way while a heavy spin-3/2 excitation of a heavy spin-1/2 quark indicated by "Rarita-Schwinger"

vector spinor Lagrangian is the most favorable choice among other beyond the standard models. As a result of this study, no significant excess is observed over expectations and a lower limit is set on a t^* quark mass of 969 GeV/c^2 at 95% confidence level. Limit calculations are performed using Asymptotic CLs method [50] with Poisson statistics. A log-normal prior is used in the integration given the background uncertainty. Figure 4.1 shows the cross section of t^* as a function of its mass. Cross section is the interaction probability per unit flux. The number of events and cross section is related with $N = \sigma \int Ldt$.

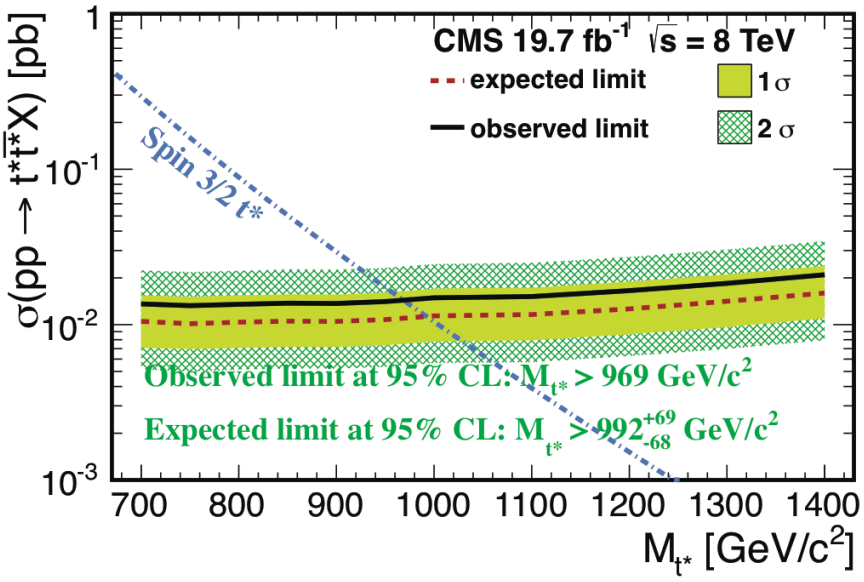

Figure 4.1: The cross section of t* while x axis is mass.

REFERENCES

[1] J. Beringer et al. (Particle Data Group), PR D86, 010001 (2012) `http://pdg.lbl.gov` , last visited 09/07/2014

[2] H. Georgi, L. Kaplan, D. Morin, and A. Schenk, "Effects of top compositeness", Phys.Rev. D51 (1995) 3888–3894, doi:10.1103/PhysRevD.51.3888, arXiv:hep-ph/9410307, last visited 09/07/2014.

[3] E. Eichten, K. D. Lane, and M. E. Peskin, "New Tests for Quark and Lepton Substructure", Phys.Rev.Lett. 50 (1983) 811–814, doi:10.1103/PhysRevLett.50.811.

[4] D. A. Dicus, S. Gibbons, and S. Nandi, "Collider production of spin 3/2 quarks", `arXiv:hep-ph/9806312`.

[5] B. Lillie, J. Shu, and T. M. Tait, "Top Compositeness at the Tevatron and LHC", JHEP 0804 (2008) 087, doi:10.1088/1126-6708/2008/04/087, arXiv:0712.3057.

[6] A. Pomarol and J. Serra, "Top Quark Compositeness: Feasibility and Implications", Phys.Rev. D78 (2008) 074026, doi:10.1103/PhysRevD.78.074026, arXiv:0806.3247.

[7] K. Kumar, T. M. Tait, and R. Vega-Morales, "Manifestations of Top Compositeness at Colliders", JHEP 0905 (2009) 022, doi:10.1088/1126-6708/2009/05/022, arXiv:0901.3808.

[8] L. Randall and R. Sundrum, "A Large mass hierarchy from a small extra dimension", Phys.Rev.Lett. 83 (1999) 3370–3373, doi:10.1103/PhysRevLett.83.3370, arXiv:hep-ph/9905221.

[9] L. Randall and R. Sundrum, "An Alternative to compactification", Phys.Rev.Lett. 83 (1999) 4690–4693, doi:10.1103/PhysRevLett.83.4690, arXiv:hep-th/9906064.

[10] Schmaltz, M. (2002). Physics beyond the standard model (theory): Introducing the little higgs. ICHEP 2002.

[11] Griffiths, D. J. Introduction to Elementary Particles (New York, USA: Wiley, 1987).

[12] D.J. Gross (1998). "Twenty Five Years of Asymptotic Freedom". Nuclear Physics B - Proceedings Supplements 74: 426–446. arXiv:hep-th/9809060. Bibcode:1999NuPhS..74..426G. doi:10.1016/S0920-5632(99)00208-X.

[13] Particle Data Group Collaboration, "Review of Particle Physics", Phys. Rev. D 86 (2012) 010001, doi:10.1103/PhysRevD.86.010001.

[14] CMS Collaboration, "Observation of a new boson at a mass of 125 GeV with the CMS experiment at the LHC", Phys. Lett. B 716 (2012), no. 1, 30 - 61, doi:10.1016/j.physletb.2012.08.021.

[15] ATLAS Collaboration, "Observation of a new particle in the search for the Standard Model Higgs boson with the ATLAS detector at the LHC", Phys. Lett. B 716 (2012), no. 1, 1 - 29, doi:10.1016/j.physletb.2012.08.020.

[16] G. Bertone, "Particle Dark Matter: Observations, Models and Searches". Cambridge University Press, 2010.

[17] D. Cline, "Dark matter in the universe: proceedings of the International Symposium on Sources and Detection of Dark Matter in the Universe : Santa Monica, California, USA, 14-16 February 1996". Nuclear physics. North-Holland, 1996.

[18] G. Bertone, D. Hooper, and J. Silk, "Particle Dark Matter: Evidence, Candidates and Constraints", arXiv:hep-ph/0404175.

[19] Cacciapaglia, G., Deandrea, A., Harada, D., and Okada, Y. (2010). Bounds and decays of new heavy vector-like top partners. JHEP, Retrieved from `http://link.springer.com/article/10.1007` , last visited 09/07/2014

[20] Hassanain, B., March-Russell, J., and Rosa, J. G. (2009). On the possibility of light string resonances at the lhc and tevatron from randall-sundrum throats. JHEP, Retrieved from `http://arxiv.org/abs/0904.4108` , last visited 09/07/2014

[21] T. Kaluza, Sitzungsber. Preuss. Akad. Wiss. Berlin (Math. Phys.) K1, 966 (1921); O. Klein, Z. Phys. 37, 895 (1926).

[22] Physics searches at the LHC. `arXiv:0912.3259` [hep-ph] 4 Sep 2010.

[23] W. Rarita and J. Schwinger, "On a theory of particles with half integral spin", Phys.Rev. 60 (1941) 61, doi:10.1103/PhysRev.60.61.

[24] B. Moussallam and V. Soni, "PRODUCTION OF HEAVY SPIN 3/2 FERMIONS IN COLLIDERS", Phys.Rev. D39 (1989) 1883–1891, doi:10.1103/PhysRevD.39.1883.

[25] CERN, "CERN faq LHC the guide." http://cds.cern.ch/record/1165534/files/CERN-Brochure-2009-003-Eng.pdf , last visited 09/07/2014

[26] CERN,"CMS." http://cms.web.cern.ch/news/cms-detector-design, last visited 09/07/2014

[27] The CMS Collaboration, "The CMS experiment at the CERN LHC," Journal of Instrumentation, vol. 3, 2008. 2.2 [JINST 3 S08004]

[28] http://www.hephy.at/user/friedl/diss/html/node26.html , last visited 09/07/2014

[29] The CMS Collaboration, "The CMS experiment at the CERN LHC", Journal of Instrumentation, Vol. 3, No. 08, pp. S08004, 2008

[30] The CMS Collaboration,"Technical Design Report of HCAL" https://cds.cern.ch/record/357153/files/CMS_HCAL_TDR.pdf, last visited 09/07/2014

[31] The CMS Collaboration,"Offline Workbook" https://twiki.cern.ch/twiki/bin/view/CMSPublic/WorkBookChapter3, last visited 09/07/2014

[32] F. Maltoni and T. Stelzer, "MadEvent: Automatic event generation with MadGraph", JHEP 0302 (2003) 027, arXiv:hep-ph/0208156.

[33] J. Pumplin et al., "New generation of parton distributions with uncertainties from global QCD analysis", JHEP 0207 (2002) 012, arXiv:hep-ph/0201195.

[34] T.Sjostrand, S.Mrenna, and P.Z.Skands, "PYTHIA 6.4 Physics and Manual", JHEP 0605 (2006) 026, doi:10.1088/1126-6708/2006/05/026, arXiv:hep-ph/0603175.

[35] J. Allison et al., "Geant4 developments and applications", IEEE Trans.Nucl.Sci. 53 (2006) 270, doi:10.1109/TNS.2006.869826.

[36] CMS Collaboration, "Particle-Flow Event Reconstruction in CMS andPerformance for Jets, Taus, and MET", CMS-PAS PFT-09-001 (2009).

[37] CMS Collaboration, "Commissioning of the Particle Flow reconstruction in Minimum Bias and Jet Events from pp Collisions at 7 TeV", CMS-PAS PFT-10-002 (2010).

[38] CMS Collaboration, "Commissioning of the Particle flow Event Reconstruction with the first LHC collisions recorded in the CMS detector", CMS Physics Analysis Summary CMS PAS PFT 10 001, CERN, (2010).

[39] CMS Collaboration, “Commissioning of the particle flow event reconstruction with leptons from J/Y and W decays at 7 TeV”, CMS Physics Analysis Summary CMS-PAS-PFT-10-003, CERN, (2010).

[40] CMS Collaboration, https://hypernews.cern.ch/HyperNews/CMS/get/top/1602.html , last visited 09/07/2014

[41] CMS Physics Object Group, “Baseline muon selection” https://twiki.cern.ch/twiki/bin/view/CMSPublic/SWGuideMuonId , last visited 09/07/2014

[42] CMS Physics Object Group, "EgammaCutBasedIdentification", https//twiki.cern.ch/twiki/bin/view/CMS/EgammaCutBasedIdentification , last visited 09/07/2014

[43] CMS Physics Object Group, "PhotonID 2012" https://twiki.cern.ch/twiki/bin/view/CMS/CutBasedPhotonID2012 , last visited 09/07/2014

[44] CMS JetMet Group, "Jet ID", https://twiki.cern.ch/twiki/bin/viewauth/CMS/JetID , last visited 09/07/2014

[45] Cacciari, M., Salam, G., P. and Soyez, G., “The anti-kt jet clustering algorithm”, Journal of High Energy Physics, Vol. 2008, No. 04, pp. 063, 2008.

[46] CMS Collaboration, https://twiki.cern.ch/twiki/bin/view/CMS/Pileup_MC_Gen_Scenarios#2012_Pileup_Scenario_s , last visited 09/07/2014

[47] Babar Collaboration, "A User’s Guide to the RooFitTools Package for Unbinned Maximum Likelihood Fitting", 2001, http://webcms.ba.infn.it/cms-software/RooFit/RooFitToolsManual.pdf , last visited 09/07/2014

[48] N. Adam et. al., "Tag and Probe Tutorial CMSSW 3 1 2", 2001.

[49] E. Asilar Y. Chang, M. Cardaci, K. Chen, M. Guler, Y. Tzeng, and S. Yu, "Search for an excited quark decaying to a top quark plus photon", CMS AN-2014/030.

[50] G. Cowan, K. Cranmer, E. Gross, and O. Vitells, "Asymptotic formulae for likelihood-based tests of new physics", The European Physical Journal C 71 (2011), no. 2,1–19, doi:10.1140/epjc/s10052-011-1554-0, arXiv:1007.1727.